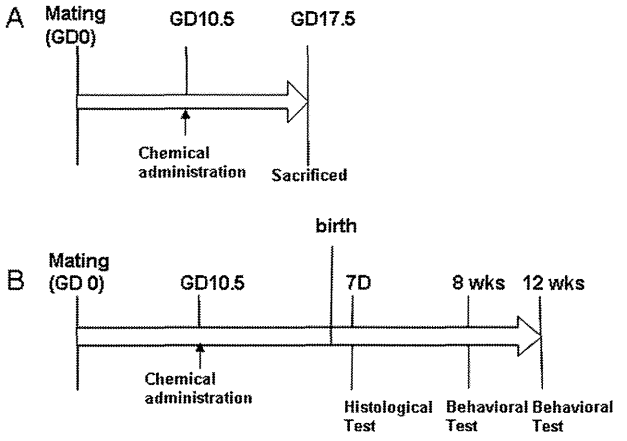

Fig. 1. Schematic experimental design. A: Regimen for prenatal exposure to permethrin and the fetal brain analysis. B: Regimen of behavioral tests.

permethrin on CNS development and neuronal transmitters at postnatal day (PND) 7 and spontaneous behavior in offspring mice at 8 and 12 weeks of age [Fig. 1(B)]. In the first experiment, at GD17.5, all the mice were sacrificed by dislocation of cervical vertebrae, and the fetuses were removed. The body weight of each fetus, without placenta and yolk sac, was measured. The fetuses were kept on iced plastic dishes, and the brains were removed. Brains were washed in phosphase buffer saline (PBS) and fixed in 4% paraformaldehyde (PFA) at 4°C overnight. The methods of the second experiment are described later.

Carbon Black Perfusion of Cerebrovasculature

Fetal mouse hearts were exposed either under anesthesia. After opening the right atrium to ambient pressure, a 26-gauge needle was inserted into the left ventricle, through which 2 mL of PBS was perfused, followed by 2 mL of carbon black ink in 4% PFA. All perfusions were performed in series at 20 rpm by using a peristaltic pump (MasterFlex, Cole-Parmer Instrument, Vernon Hills, IL). The brains were carefully removed, and the CW anatomy was visualized by using a stereomicroscope with a cooling charge-coupled device image sensor (CCD) camera (Olympus, Tokyo, Japan).

Whole-Mount Immunohistochemistry

Fixed brains were washed in PBS with 0.2% Triton-X for 30 min, permeabilized in PBS with 50% DMSO for 20 min and washed three times in PBS with 0.2% Triton-X for 30 min. The brains were incubated in PBS with 5% normal goat serum to block nonspecific immunoreactivity. After 1 h of blocking, the primary immunoreaction was performed in PBS with 5% normal goat serum and 1:200 rat anti-CD31 (PECAM-1) antibody (MEC 13.3; BD Pharmingen, San Diego, CA) overnight at 4°C. Brains were washed three times in PBS with 0.2% Triton-X for 30 min, and blocking for the secondary immunoreaction was carried out in PBS with 5% normal goat serum. The secondary immunoreaction was performed in PBS with 5% normal goat serum and 1:200 antirat IgG antibody-conjugated Alexa 546 (Invitrogen, Carlsbad, CA). After washing three times in PBS, images of the anterior half of the CW area were obtained using a cooling CCD camera under fluorescent microscopy (Olympus, Tokyo, Japan). Photographs of the whole brain were also obtained under a stereomicroscope (Olympus) to measure the length of the anterior–posterior axis. The frequencies of the abnormal location were calculated as the ratio of the number of fetus with the abnormal location versus the sample number of in each exposure group.

Histological and Anatomical Analyses

Histological and anatomical observation and image analyses of cerebrovasculature in the brain were performed using a stereo microscope (Olympus SZX16 Macroview, Sinjuku, Tokyo) and image-processing software (WinRoof, Mitani Corporation, Fukui, Japan). For the GD17.5 fetal brain, the length of the anterior–posterior axis of the whole brain, the length of the anterior cerebral arteries (ACA) or anterior communicating arteries (AComA), and the number of branches of the ACA or AComA were measured. For histological analysis of cortex layers at the Bregma, brains of mice at PND7 were fixed with 10% formalin solution, then washed in 70% ethyl alcholo-xylene, and embedded in paraffin. Those brains were cut in the coronal plane at 10 μm. Sections were collected every 50 μm, thaw-mounted onto coated slides, and stained with 0.5% Cresyl violet. The thickness of the cortical layers in the lateral part of secondary visual cortex (V2L) and the thickness of pyramidal cell layers (Py) in hippocampus and granular layers in the dentate gyrus (GrDG) were quantitatively measured at the -2 mm place from the Bregma position of brain.

Measurement of Monoamines by High-Performance Liquid Chromatography

The monoamines and their metabolites were measured using high-performance liquid chromatography (HPLC) with electrochemical detector. At PND7, the brain after removing cerebellum was rapidly dissected out, weighted, and frozen at -80°C until assay. Each frozen brain was homogenized by ultrasonic irradiation in 2 mL of 0.2 M perchloric acid/0.1 mM EDTA solution containing isoproterenol as an internal standard. The homogenates were placed on ice for 30 min and spun at 20,000 $\times$ g for 10 min

at 4°C. The supernatants were filtered through a syringe filter unit (DISMIC-3; Advantec, Japan), their pH was adjusted to 3.0 by adding 1 M sodium acetate, and then they were injected into a HPLC system (Shimadzu, Japan) equipped with an ODS column (Eicompak SC5-ODS; 3 mm i.d. × 150 mm; Eicom, Japan) and an electrochemical detector (EDC-100; Eicom) with the potential set at + 750 mV. The mobile phase was 0.1 M citric acid/0.1 M sodium acetate, pH 3.5, containing sodium-1-octansulfonate (190 μg/mL), EDTA-2Na (5 μg/mL), and 13% methanol. The flow rate was set at 0.25 mL/min.

Behavioral Tests

For behavioral tests, pregnant ICR mice at GD10.5 were administrated permethrin dissolved in corn oil at a dose of 0, 2, or 50 mg/kg. Three litters were used in each group. The mean body weight of all groups was approximately equal. At 7 days after parturition, three males and three females were reserved from each litter. Motility was examined at 8 and 12 weeks using selected items from a modified-SHIRPA test (Rogers et al., 2001; Masuya et al., 2005; Jin et al., 2008a). We tested body weight, body position, grooming, locomotor activity, transfer arousal, trunk curl, contact righting reflex, and negative geotaxis using a clear perspex cylindrical viewing jar (14-cm diameter × 18-cm height), a clear perspex arena (60-cm length × 37-cm width × 18-cm height with a the floor marked with 15 squares), and a grid (40 cm × 20 cm with 12-mm mesh) at 8 and 12 weeks of age. For quantitative analysis of motor activity, we counted the number of leaning-against wall events for 5 min in the viewing jar to test body-position activity, and we counted the number of squares in the floor of the arena that the mice ran through for 1 min to test locomotor activity. After the test at 12 weeks of age, mice were sacrificed, and their brains were removed. Brains were fixed in 4% PFA after being weighed. After overnight fixation, the brains were photographed under a dissection microscope and used in image analysis.

Statistical Analyses

Statistical analysis was performed using SAS software (version 9.1 with Enterprise 4.0, SAS Institute, Cary, NC). Differences among doses were determined for each endpoint. Data were tested for normality using the Shapiro–Wilk test and for homogeneity using Bartlett's test for experiments using multiple dose levels of a test chemical. When the data were found to be homogeneous ($P > 0.05$), Dunnett's multiple analysis was performed. If the data were from experiments using a single dose level of a test chemical and the initial variance of the data were homogeneous, the data were analyzed by the Student's t test. Each evaluation was by two-tailed tests with 0.05, 0.01, or 0.001 as the levels of significance.

TABLE I. Effects of prenatal exposure to thalidomide or permethrin on dam body weights, litter sizes and fetal body weights at GD17.5

Group	Number of Dams	Average Body Weight of Dams	Litter Size	Fetal Body Weight
Control				
Total	5	68.1 ± 1.7	19.4 ± 0.7	0.775 ± 0.005
Male			10.2 ± 1.2	0.788 ± 0.007
Female			9.2 ± 0.5	0.762 ± 0.007
Thalidomide (150 mg/kg)				
Total	4	62.7 ± 1.8	16.0 ± 0.7	0.787 ± 0.006
Male			9.5 ± 1.0	0.797 ± 0.008
Female			6.5 ± 0.6	0.773 ± 0.007
Permethrin (10 mg/kg)				
Total	5	62.4 ± 1.1*	15.6 ± 0.9*	0.827 ± 0.022*
Male			6.8 ± 0.7*	0.846 ± 0.029
Female			8.8 ± 1.2	0.811 ± 0.031

*$P < 0.05$ from correspondent control.

RESULTS

Detection of Vascular Malformation in Fetus Brains Prenatally Exposed to Thalidomide or Permethrin

The effects of prenatal exposure to chemicals on dam body weights, litter sizes, and fetal body weights at GD17.5 were shown in Table I. Mice were prenatally exposed to corn oil as vehicle, thalidomide, or permethrin. Thalidomide was used as positive controls that induce abnormal patterning of the cerebral arteries in the CW and its surrounding arteries. Permethrin exposures significantly decreased the body weight of dams and litter sizes, but increased the fetal body weight. As a positive agent, thalidomide did not show significant alterations for the body weight of dams, litter sizes, and the fetal body weight.

Fetal brains were analyzed to determine alterations in the development of cerebral arteries in the CW [Fig. 2(A)]. Figure 2(A) shows a schematic picture of arteries of the CW in the fetal mouse brain; the left side of the brain represents normal patterning of cerebral arteries, and the right side depicts abnormal patterning. For the GD17.5 fetal brain, the half length of the anterior–posterior axis of the whole brain, the length of the ACA [ab in Fig. 2(A)] or the length AComA [bc in Fig. 2(A)], and the number of branches of the ACA or AComA were measured as shown in Figure 2(A). These observations were summarized in Table II. When more than three branches in the right and left ACA or AcomA were observed, the vascular patterns were assessed as abnormal locations [Fig. 2(C–F)]. Prenatal exposure to thalidomide significantly increased frequencies of abnormal locations in the right ACA [Fig. 2(C,D)]. In

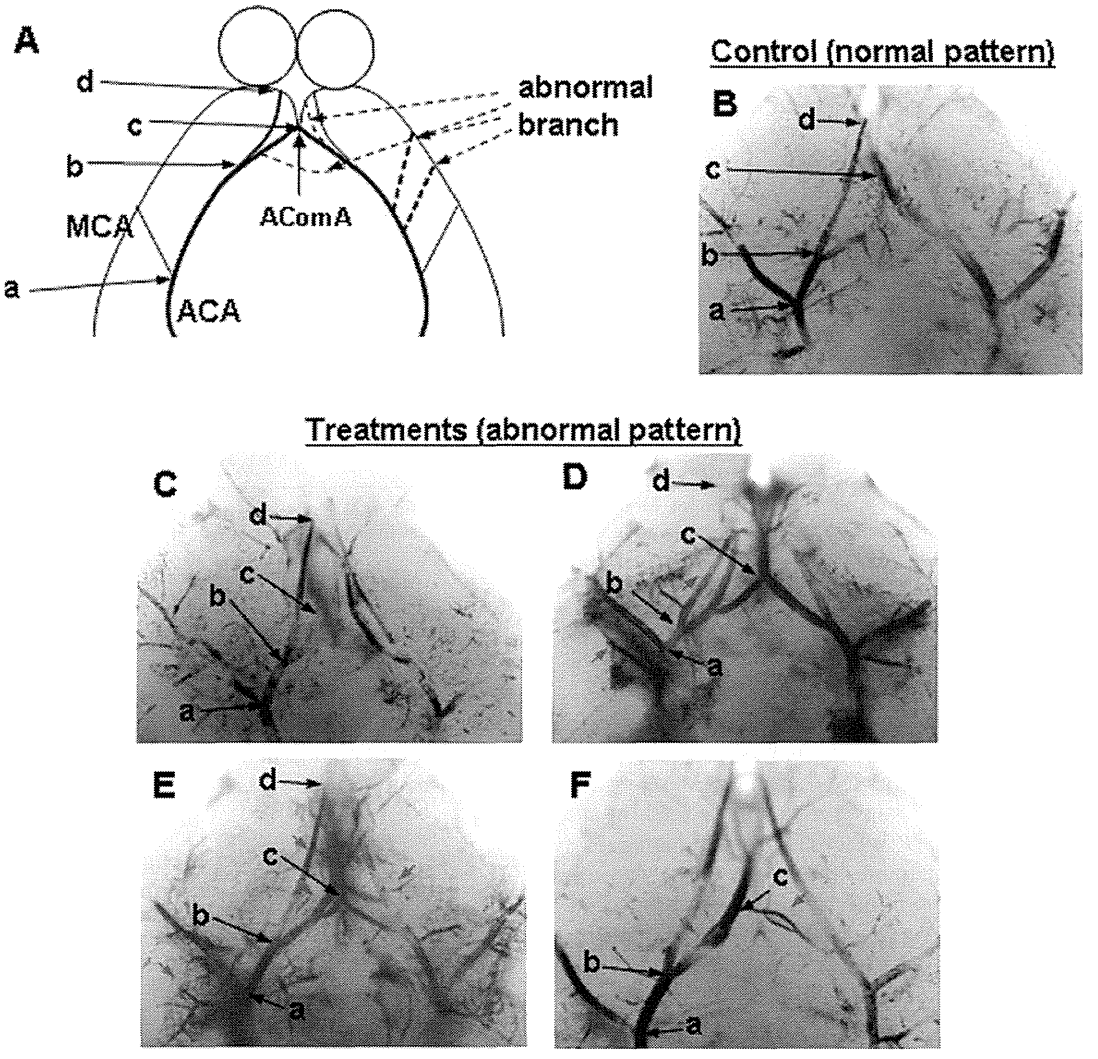

Fig. 2. Drawing and representative photographs of the anterior half of CW in the fetal mouse brain. Drawing (A), control (B), 150 mg/kg thalidomide (C and D) and 10 mg/kg permethrin (E and F) groups. a, b, c, and d in the drawing and each photograph indicate the branching point of MCA and ACA, the branching point of AcomA and ACA, the fusion point of AcomA, and the end of ACA, respectively. Prenatal exposure to thalidomide or permethrin causes various malformations of the CW of fetal brains. Vascular networks were filled with a fourfold dilution of Chinese liquid ink. Arrows indicate malformation sites detected. [Color figure can be viewed in the online issue, which is available at wileyonlinelibrary.com.]

the case of permethrin, frequencies of abnormal locations in the AcomA [Fig. 2(E,F)] were increased. Different patterning of the CW was observed between thalidomide and permethrin-exposed fetal brain.

Dose-Range Effects of Permethrin on Cerebral Arteries in CW of the Mouse Brain

To confirm the effects of prenatal exposure to permethrin on cerebral arteries in the CW, its dose-response relationship was assessed. Branching patterns in the CW of brains were detected by immunohistochemical examinations, which were performed with anti-PECAM-1 antibody. Typical immunohistochemical observations in each group were shown in Figure 3. As we mentioned previously, in the control group, ACAs were connected by AComAs that were fused on the anterior side of the optic chiasma. Major cerebral arteries including the MCA and ACA showed few small branches in the control group [Fig. 3(A)]. In contrast, branching of cerebrovasculars in the CW of brains isolated from permethrin-treated fetuses [Fig. 3(B–E)] showed no

TABLE II. Prenatal exposure to thalidomide or permethrin causes various malformations of the CW of fetal brains

Group	Number of Tested Fetus	Frequencies of Abnormal Locations			*P* Value of the Chi Square Test		
		Right ACA	Left ACA	AcomA	Right ACA	Left ACA	AcomA
Control							
Total	25	0.20	0.32	0.24	–	–	–
Male	14	0.21	0.36	0.21	–	–	–
Female	11	0.18	0.27	0.30	–	–	–
Thalidomide (150 mg/kg)							
Total	21	0.48*	0.38	0.24	0.047	0.666	0.988
Male	11	0.45	0.36	0.21	0.201	0.973	0.943
Female	10	0.50	0.40	0.30	0.122	0.537	0.916
Permethrin (10 mg/kg)							
Total	25	0.28	0.44	0.96**	0.508	0.382	0.009
Male	13	0.31	0.46	0.92*	0.580	0.581	0.037
Female	12	0.25	0.42	0.92	0.692	0.469	0.122

*$P < 0.05$ and **$P < 0.001$ from correspondent control. More than three branches in the right and left ACA or AcomA were assessed as abnormal locations of the CW area. The frequencies of the abnormal location were calculated as the ratio of the number of fetus with the abnormal location versus the sample number of fetus in each exposure group.

AComAs and many small and slender branches from the ACA. In addition, insufficient fusion of the AComAs was also observed in some cases as shown in Figure 3(C,E).

To quantify these observations in terms of the permethrin influence, we determined the number of branches in the area [bc as shown in Fig. 2(A)] of the AComA significantly increased in fetal brains exposed to permethrin at a dose of 2 ($P < 0.05$), 10 ($P < 0.001$), 50, or 75 mg/kg ($P < 0.01$) [Fig. 4(A)]. Furthermore, the length of the AComA was reduced significantly in the fetuses exposed to permethrin at a dose of 10 mg/kg ($P < 0.05$) [Fig. 4(B)] while the lengths of the ACA [ab and bd as shown in Fig. 2(A)] or branch numbers on it was neither affected by the prenatal exposure to permethrin. In summary, the abnormalities of CW were caused by 2 mg/kg of permethrin, which the lowest dose we experimented, and reached the plateau at 10 mg/kg. Therefore, we use the samples from the one exposure group, 50 mg/kg, in histological analysis and measurement of neurotransmitter.

Effects of Permethrin on Histological Observations and Neurotransmitter at Early PN Development

We next investigated how prenatal exposure to 50 mg/kg of permethrin influences the processes of neuronal

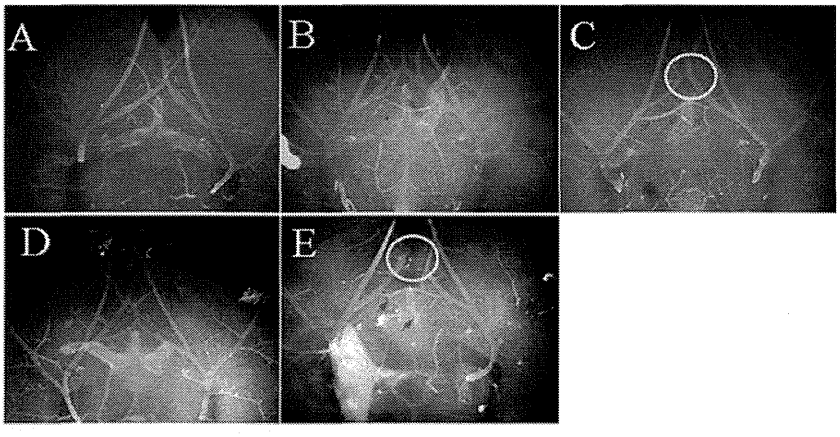

Fig. 3. Arteries of CW of fetal brains are affected by prenatal exposure to permethrin. Representative photographs of the anterior half of the CW of fetal brains; prenatal exposure to permethrin causes various malformations of the CW. Control (A), 2 mg/kg permethrin (B), 10 mg/kg permethrin (C), 50 mg/kg permethrin (D), and 75 mg/kg permethrin (E) groups. Arrows and circles indicate malformation sites detected. [Color figure can be viewed in the online issue, which is available at wileyonlinelibrary.com.]

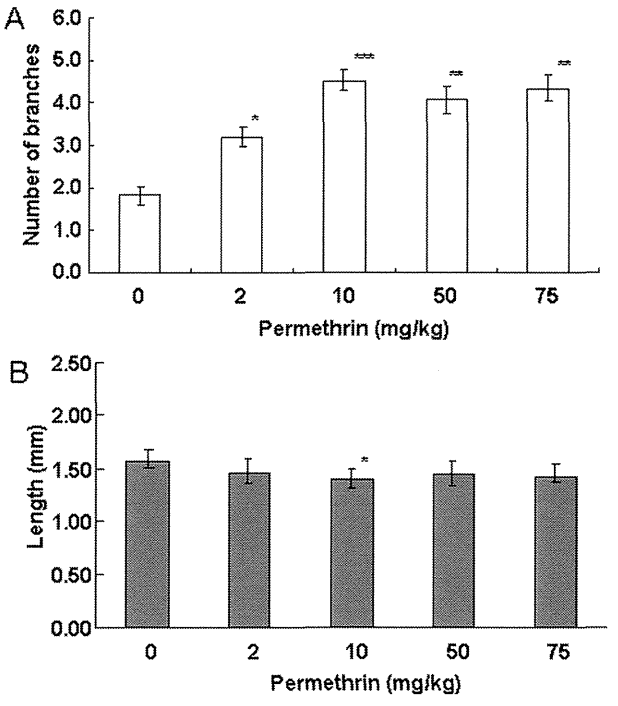

Fig. 4. Prenatal permethrin exposures alter vascular pattern in the CW area. Number of branches from the anterior half of ACA [bd as shown in Fig. 2(A) picture] and the length of AcomA [bc as shown in Fig. 2(A) picture] were measured. Dose-response relationship between the permethrin exposure and abnormal branches (A) in the observed area and the length of AcomA (B). Values are mean ± SE. $^{*}P < 0.05$; $^{**}P < 0.01$; $^{***}P < 0.001$.

commitment and differentiation during early PN development. Because it was known that prenatal stress alters spine density and dendritic length and hippocampus neurons in rat offspring (Tseng et al., 2008; Lu et al., 2009), we assessed the thickness of cortical layers in the V2L, Py, and GrDG in the hippocampus. Notably, the significant differences were found reduced layer I, Py, and GrDG in mice prenatally exposed to permethrin in compared to control [Fig. 5(E,F)]. However, there were no significant differences for the other layers (II–VI) and the thickness between the hippocampus and the dentate gyrus near the Bregma [Fig. 5(E,F)]. These data indicate that prenatal exposure to permethrin influenced CNS development at the later PN period.

Second, we sought to determine whether influences of permethrin to CNS development were due to premature contents of neurotransmitters. Levels of norepinephrine (NA), dopamine (DA), DOPAC, HVA, 5HT, and 5HIAA at PND7 were determined in controls and the mice after prenatal exposure to permethrin (Fig. 6). NA and DA in the permethrin-exposed mice were significantly increased in compared to control. However, there were no significant differences in the other neurotransmitters between controls and the exposed mice. Together, these results indicate that prenatal exposure to permethrin affects cortical layers and development of dopaminergic and adrenergic neurons in the hippocampus region.

Effects on Motor Behavior in Adulthood

To evaluate behavioral activity during the adulthood of mice prenatally exposed to permethrin, the body-position test and the open-field arena test were conducted at 8 and 12 weeks of age. In the body-position test, no difference was detected in either females or males at 8 weeks of ages. However, at 12 weeks of age, the number of leaning-against wall events for the body-position test that occurred in the 5-min observation period in males was significantly decreased at a dose of 2 mg/kg (Fig. 7). For the confirmation of the effect of permethrin on locomotor activity, motor behavior was observed in an open-field arena for 1 min. In the arena test, the number of squares that the mice passed through significantly decreased at 50 mg/kg of permethrin in males, but not in females. Similarly, at 12 weeks of age, 2 mg/kg permethrin significantly decreased the locomotor activity of male mice, but not female mice (Fig. 8); however, at 50 mg/kg of permethrin, the decrease was not significant because of marked data variation.

Prenatal exposure to permethrin did not affect body weight at 8 and 12 weeks of age. No difference was detected in the ratio of brain/body weight in both males and females. The length of the CW also was not affected (data not shown).

DISCUSSION

In mouse brain development, the internal carotid arteries can be recognized at GD 10.5, which is when the pregnant mice were administered permethrin in the present study. Internal carotid arteries give rise to the ACA, from which the AComA branch. At the same time, the posterior cerebral arteries and posterior communicating arteries branch from the basilar artery, which is derived from the vertebral arteries. All the components of the CW are formed by GD13.5 (Kaufman, 1995). In neural tissues, the cephalic region of the neural tube begins developing rapidly at GD10.5, and the fetal brain is formed by GD13.5. Therefore, GD10.5 is thought to be the critical window for brain vascular development. Taking into consideration brain vascular development, this study was conducted using exposure to permethrin on GD10.5. Our results demonstrated that the prenatal exposure to permethrin altered patterning of the vascular formation in portions of the CW in fetal mice, including a shortening of the AComA and an increased number of small branches of the AComA. In some cases examined in this study, insufficient fusion of

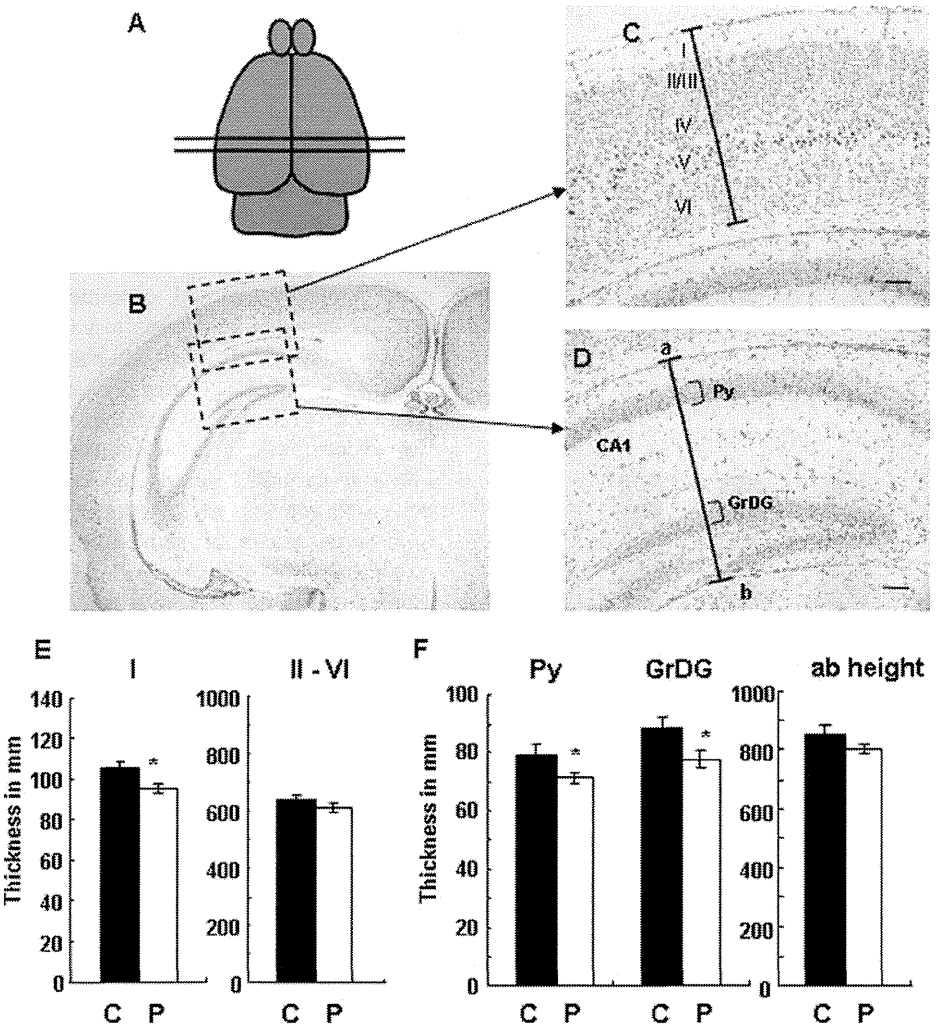

Fig. 5. Morphological alteration of the developing midbrain in the mice prenatally exposed to 50 mg/kg of permethrine. Quantitative analysis reveals a significant reduction of cortical layers and hypocampus in the permethrine-exposed brain in compared with the vehicle control at PND7. A: The schematic drawing of the mouse brain. B: Cresyl violet staining of cross-sectional brain at PND7. Squares with dot lines indicate area that quantitatively analyzed. C: Cortical layers in the lateral part of secondary visual cortex at the −2 mm place from the Bregma position of brain. D: Pyramidal cell layers (Py) in hyppocampus and granular layers in the dentate gyrus (GrDG). D: Quantitative analysis of cortical layers. E: Quantitative analysis of Py layers, GrDG layers, and the height (ab) between hyppocampus and the dentate gyrus. Data values represent mean ± SE for 12–16 individual samples per each group. $^*P < 0.05$. [Color figure can be viewed in the online issue, which is available at wileyonlinelibrary.com.]

the AComA was observed. Furthermore, the adult behavioral examination revealed that prenatal exposure to permethrin caused changes in motor behavior.

In this study, the lowest dose 2 mg/kg showed significant influences on vascular development in fetus and adult offspring behaviors, indicating that prenatal exposure to permethrin is more susceptible rather than the postnatal exposure. Considering doses of permethrin used in this study, we used 2, 10, 50, and 75, which are 1/250, 1/50, 1/10, and 1/6.7 of the oral LD50 of mice (Miyamoto, 1976), because less than 2mg/kg permethrin increased levels of dopamine transporter protein in the striatum of adult mice (Bloomquist et al., 2002) and higher doses of permethrin induced a significant risk to the offspring following treatment of F0-mice before mating (Farag et al., 2006). Although there is no direct evidence for absorption to fetus

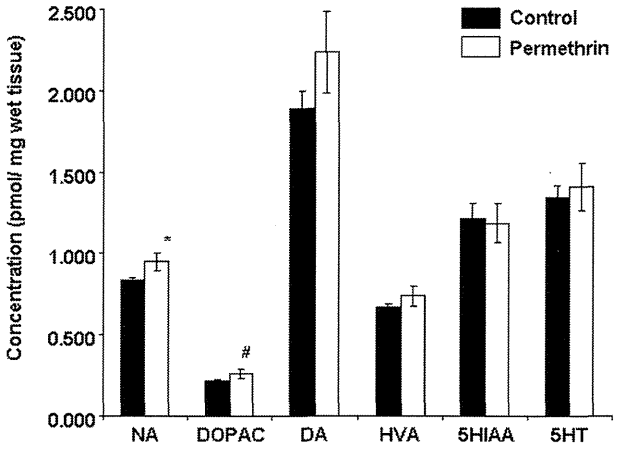

Fig. 6. Levels of norepinephrine (NA), dopamine (DA), 3,4-dihydroxyphenylacetic acid (DOPAC), and 3-methoxy-4-hydroxyphenylacetic acid (HVA) homovanillic acid (HVA), serotonin (5HT), 5-hydroxyindoleacetic acid (5HIAA), in mid brain of mice from control group, and permethrin-treated groups (50 mg/kg). Data are presented as mean ± SE for six mice per each group. *$P < 0.05$ versus control (C).

from the dam in rodent experiments, human cord blood concentrations of permethrin could be detected about 30 ng/mL nonlipid adjusted geometric mean (Neta et al., 2010). These levels of permethrin in cord blood were associated with the decrease of the anti-inflammatory cytokines IL-10 (Neta et al., in press). Therefore, it becomes crucial to verify the probable absorbed quantity of permethrin or other pyrethroids if vulnerable populations such as pregnant women would be exposed to higher permethrin or pyrethroids.

Prenatal exposure to teratogens such as MAM or thalidomide at nonteratogenic doses has been reported to produce cortical development malformation (Hallene et al., 2006; Bassanini et al., 2007). Prenatal exposure to thalidomide at GD15 induced significant morphological alterations in the cortical and hippocampal regions of rats along with vascular malformations and a leaky blood–brain barrier. These malformations were suggested due to inhibition of vascular development and neurogenesis by MAM or thalidomide. In the present study, the shorter length and the increased number of small branches were also detected in the GD10.5 thalidomide-treated group as a positive control although the positions of vascular lesions were different from those in the permethrin group. Thalidomide also inhibits vasculogenesis in various cancer and reumatitis (Sleijfer et al., 2004). Therefore, angiogenetic blockers commonly may play an inhibitory role in cerebular vascular development during the prenatal period.

The failure of fusion was similar to the abnormal formation of ACA observed in rats treated with MAM (Bardosi et al. 1985a,b, 1987; Bassanini et al., 2007). Thus, our observations *in vivo* suggest that permethrin exhibits vascular toxicity, leading indirectly to an inhibition of brain development. To examine the inhibitory action of permethrin in cerebral artery development, the *in vitro* tubular formation assay, using human brain microvascular endothelial cells, was performed in our laboratory. A concentration of 10^{-6} M or 10^{-5} M of permethrin decreased the distance between branches and increased unattached branches (data not shown). These *in vitro* results are consistent with our *in vivo* mouse study, suggesting that permethrin acts directly on endothelial cells and disrupts angiogenesis in the fetal brain. However, other hypotheses must be considered: (1) the neurotoxicity of permethrin directly inhibited brain development and then follows inhibitory of vascular development and (2) the dual action of permethrin, including neurotoxicity and vascular toxicity, inhibited directly brain development. Another possibility of effects of prenatal exposure to permethrin should be considered to be nutritional factors or alterations of general metabolisms from dams, because body weights of dams and litter sizes were significantly decreased, and fetal body weights at GD17.5 were significantly increased (Table I). This point for nutritional factors needs further studies to clear relationships with vascular developments in fetal brain.

On the other hand, regions of the observed vascular abnormality were different between thalidomide and permethrin. Although thalidomide influenced the ACA region, permethrin caused abnormalities of AcomA. It indicated that permethrin affected on vascular later than thalidomide, because the formation of AcomA follows to the ACA formation. A possible hypothesis is that the different mechanisms of the chemicals might result in such a time lag. But it is unlikely because *in vitro* tubular formation assay revealed the similar effect of thalidomide and permethrin at the same timing (data not shown). Another possible hypothesis is that the different kinetics of them in the pregnant mice and the fetus produced such a time lag. The longer time might need to reach to the toxic concentration of permethrin in the fetal brain than thalidomide. However, at least in our knowledge, no information is available about the kinetics of permethrin in the pregnant mice and the fetus. Further research is needed on the similarities or differences of permethrin and thalidomide.

Midbrain DA neurons send one of their largest cortical projections to the superficial layers of the lateral entorhinal cortex where they target principal cell islands (Björklund, 1984; Fallon, 1987). The large dopaminergic projection to the prefrontal cortex is known to regulate cellular processes related to working memory (Goldman-Rakic, 1999), and dopaminergic inputs to the lateral entorhinal cortex are also likely to affect mechanisms of sensory and mnemonic function (Seamans and Yang, 2004).

Previous studies reported that permethrin inhibits the activities of various neurons *in vitro*, including neurons of the frontal cortex, spinal cord (Shafer et al., 2008), and

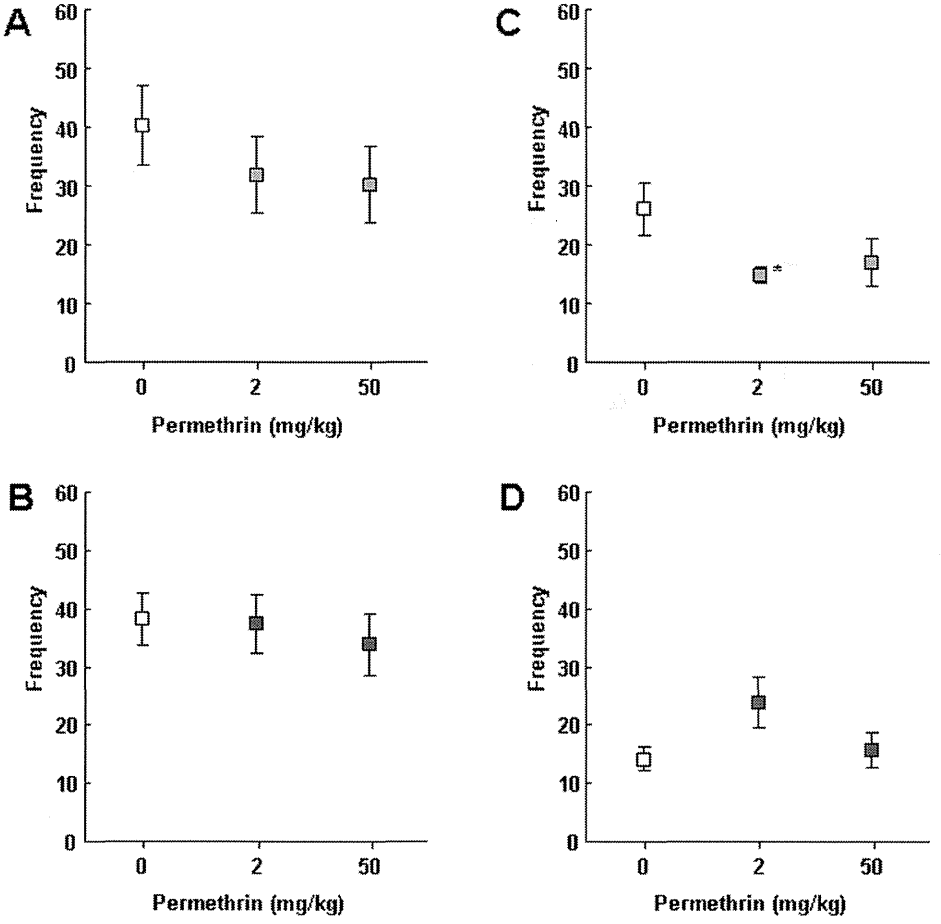

Fig. 7. Prenatal exposure to permethrin affects locomotor activity, as assessed using the body-position test. A: Male at 8 weeks of age. B: Female at 8 weeks of age. C: Male at 12 weeks of age. D: Female at 12 weeks of age. Data values represent mean ± SE. $^*P < 0.05$.

hippocampus (Meyer et al., 2008) as well as cerebellar granule cells in culture (Imamura et al., 2000). In concordance with those reports, our current studies showed the NA and DA concentrations in mice prenatally exposed to 50 mg/kg of permethrin were significantly decreased concurrently with a decreasing cortical layers and Py and GrDG in hippocampus (Figs. 5 and 6). These alterations at the early postnatal period of PND7 indicate a weak suppression of CNS development. In permethrin-treated adult animals, abnormalities of the dopaminergic system and degeneration of dopaminergic neurons have been observed, indicating a possible involvement of permethrin in Parkinson's disease (Karen et al., 2001; Bloomquist et al., 2002; Jortner, 2006). The prenatal exposure to permethrin before the mating decreased motor activities such as self-righting reflex, geotaxis reflex, cliff-avoidance reflex, swimming performance, open-field activity, and social interaction in F_1 mouse pups (Farag et al., 2006). Thus, the neurotoxic activity of permethrin may influence histological neurogenesis and CNS-related behaviors. The adult behavioral examination in our present study revealed that prenatal exposure to permethrin caused changes in motor behavior (Figs. 7 and 8). Taken together, our observations suggest that prenatal exposure to permethrin results in an insufficient development of the brain because of either the vascular toxic activity or neurotoxicity or both.

For the motor behavioral tests in the present study, we used a modified-SHIPRA test for screening. Quantitative analysis was performed by counting the number of leaning-against wall events and the number of squares passed through in the body position and arena test, respectively, to clarify the influences of the permethrin exposure. At 8 weeks of age, prenatal exposure to 50 mg/kg permethrin in the males resulted in significantly decreased locomotor activity in the arena test. At 12 weeks of age, prenatal exposure to 2 mg/kg permethrin significantly decreased locomotor activity both in the body-position test and the arena test in males, but not in females. In female mice, a significant increase was observed in the body-position test at 2 mg/kg permethrin (Figs. 7 and 8).

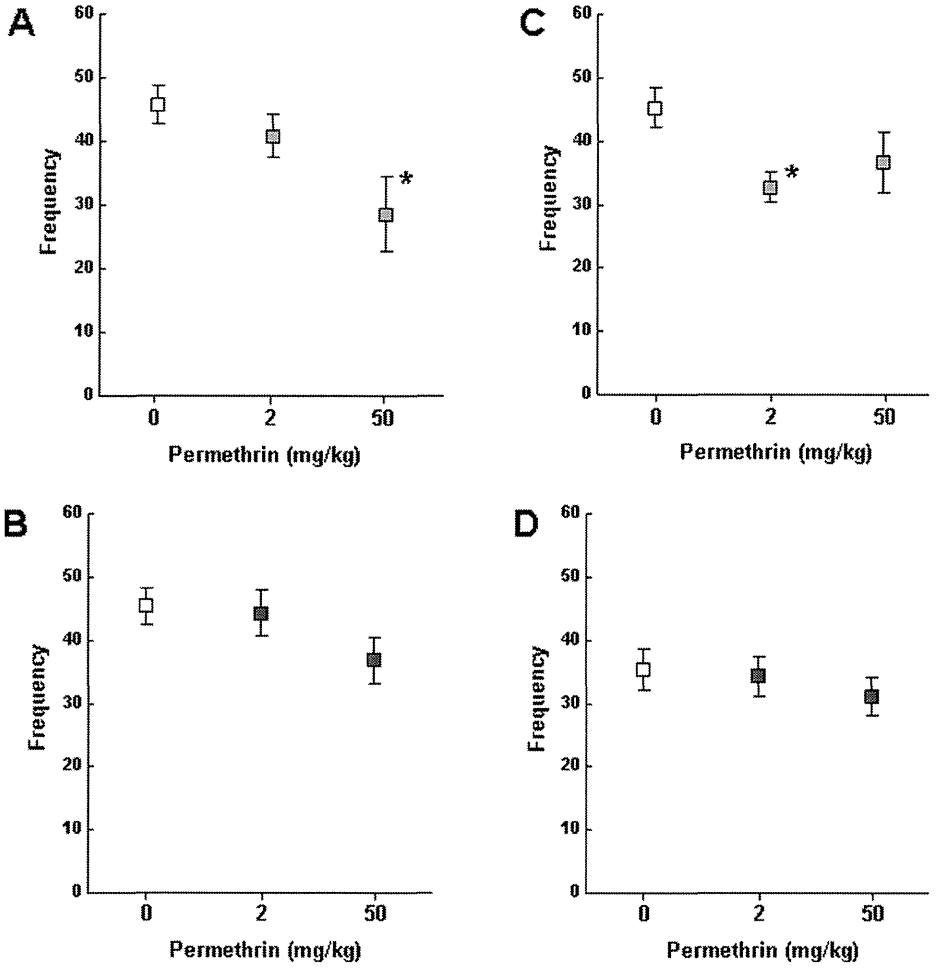

Fig. 8. Prenatal exposure to permethrin affects locomotor activity, as assessed using the arena test. A: Male at 8 weeks of age. B: Female at 8 weeks of age. C: Male at 12 weeks of age. D: Female at 12 weeks of age. Data values represent mean ± SE. *$P < 0.05$.

These sex and age differences may relate to sexual maturation. Sexual differentiation in the mouse brain is critical in fetal and perinatal periods and depends on the specific activity of androgen in the brain. Because many studies have indicated an estrogenic or antiandrogenic activity of permethrin (Garey and Wolff, 1998; Kim et al., 2004; Kojima et al., 2005; Dhooge et al., 2006; McCarthy et al., 2006; Jin et al., 2008b), it is possible that permethrin exposure *in utero* disrupts sexual differentiation of the brain and affects behavior during the period of sexual maturation.

Although prenatal exposure to permethrin on GD10.5 caused abnormal motor activity in mice at 12 weeks, brains grew to a normal size, and vascular malformations in the CW were not detected at our gross observation (data not shown). These results suggest that the recovery of morphological malformations of the vasculature during the postnatal period enabled normal growth of the brain, even though the vascular malformation had occurred during early brain development. However, the mice were unable to recover from the functional abnormality resulting from insufficient early development of the brain.

In this study, we showed that permethrin exposure *in utero* caused fetal brain vascular malformations and changes in motor behavior in adult mice. Although the relation between these abnormalities is unclear, our data show that prenatal exposure to permethrin can be a risk for health in adulthood. However, toxicological information concerning prenatal exposure to permethrin is insufficient. Further research is needed on the effect of prenatal exposure to permethrin.

REFERENCES

Bardosi A, Ambach G, Friede RL. 1985a. The angiogenesis of micrencephalic rat brains caused by methylazoxymethanol acetate. I. Superficial venous system. A quantitative analysis. Acta Neuropathol 66:253–263.

Bardosi A, Ambach G, Friede RL. 1985b. The angiogenesis of micrencephalic rat brains caused by methylazoxymethanol acetate. II. Superficial and basal arterial system. Acta Neuropathol 68:59–64.

Bardosi A, Ambach G, Hann P. 1987. The angiogenesis of the micrencephalic rat brains caused by methylazoxymethanol acetate. III. Internal angioarchitecture of cortex. Acta Neuropathol 75:85–91.

Bassanini S, Hallene K, Battaglia G, Finardi A, Santaguida S, Cipolla M, Janigro D. 2007. Early cerebrovascular and parenchymal events following prenatal exposure to the putative neurotoxin methylazoxymethanol. Neurobiol Dis 26:481–495.

Björklund A, Lindvall O. 1984. Dopamine-containing systems in the CNS. In: Björklund A, Hökfelt T, editors. Handbook of Chemical Neuroanatomy. Amsterdam: Elsevier. pp 55–122.

Bloomquist JR, Barlow RL, Gillette JS, Li W, Kirby ML. 2002. Selective effects of insecticides on nigrostriatal dopaminergic nerve pathways. Neurotoxicology 23:537–544.

Cantalamessa F. 1993. Acute toxicity of two pyrethroids, permethrin, and cypermethrin in neonatal and adult rats. Arch Toxicol 67:510–513.

Cattaneo E, Reinach B, Caputi A, Cattabeni F, Di Luca M. 1995. Selective in vitro blockade of neuroepithelial cells proliferation by methylazoxymethanol, a molecule capable of inducing long lasting functional impairments. J Neurosci Res 41:640–647.

Dhooge W, Arijs K, D'Haese I, Stuyvaert S, Versonnen B, Janssen C, Verstraete W, Comhaire F. 2006. Experimental parameters affecting sensitivity and specificity of a yeast assay for estrogenic compounds: Results of an interlaboratory validation exercise. Anal Bioanal Chem 386:1419–1428.

Fallon JH LS. 1987. Monoamine innervation of cerebral cortex and a theory of the role of monoamines in cerebral cortex and basal ganglia. In: Jones EG, Peters A, editors. Cerebral Cortex. New York: Plenum. pp 41–127.

Farag AT, Goda NF, Mansee AH, Shaaban NA. 2006. Effects of permethrin given before mating on the behavior of F1-generation in mice. Neurotoxicology 27:421–428.

Gabbianelli R, Falcioni G, Nasuti C, Cantalamessa F. 2002. Cypermethrin-induced plasma membrane perturbation on erythrocytes from rats: Reduction of fluidity in the hydrophobic core and in glutathione peroxidase activity. Toxicology 175: 91–101.

Gabbianelli R, Nasuti C, Falcioni G, Cantalamessa F. 2004. Lymphocyte DNA damage in rats exposed to pyrethroids: Effect of supplementation with Vitamins E and C. Toxicology 203: 17–26.

Garey J, Wolff MS. 1998. Estrogenic and antiprogestagenic activities of pyrethroid insecticides. Biochem Biophys Res Commun 251:855–859.

Gillette JS, Bloomquist JR. 2003. Differential up-regulation of striatal dopamine transporter and alpha-synuclein by the pyrethroid insecticide permethrin. Toxicol Appl Pharmacol 192:287–293.

Goldman-Rakic PS. 1999. The ''psychic'' neuron of the cerebral cortex. Ann NY Acad Sci 868:13–26.

Gorell JM, Johnson CC, Rybicki BA, Peterson EL, Richardson RJ. 1998. The risk of Parkinson's disease with exposure to pesticides, farming, well water, and rural living. Neurology 50: 1346–1350.

Haddad RK, Rabe A, Dumas R. 1972. Comparison of effects of methylazoxymethanol acetate on brain development in different species. Fed Proc 31:1520–1523.

Hallene KL, Oby E, Lee BJ, Santaguida S, Bassanini S, Cipolla M, Marchi N, Hossain M, Battaglia G, Janigro D. 2006. Prenatal exposure to thalidomide, altered vasculogenesis, and CNS malformations. Neuroscience 142:267–283.

Heldin CH. 2004. Development and possible clinical use of antagonists for PDGF and TGF-β. Ups J Med Sci 109:165–178.

Imamura L, Hasegawa H, Kurashina K, Hamanishi A, Tabuchi A, Tsuda M. 2000. Repression of activity-dependent c-fos and brain-derived neurotrophic factor mRNA expression by pyrethroid insecticides accompanying a decrease in Ca^{2+} influx into neurons. J Pharmacol Exp Ther 295:1175–1182.

Jin HG, Yamashita H, Nakamura T, Fukuba H, Takahashi T, Hiji M, Kohriyama T, Matsumoto M. 2008a. Synphilin-1 transgenic mice exhibit mild motor impairments. Neurosci Lett 445:12–17.

Jin Y, Wang W, Xu C, Fu Z, Liu W. 2008b. Induction of hepatic estrogen-responsive gene transcription by permethrin enantiomers in male adult zebrafish. Aquat Toxicol 88:146–152.

Johnston MV, Coyle JT. 1979. Histological and neurochemical effects of fetal treatment with methylazoxymethanol on rat neocortex in adulthood. Brain Res 170:135–155.

Jones EG, Valentino KL, Fleshman JW Jr. 1981. Adjustment of connectivity in rat neocortex after prenatal destruction of precursor cells of layers II-IV. Brain Res 254:425–431.

Jortner BS. 2006. The return of the dark neuron. A histological artifact complicating contemporary neurotoxicologic evaluation. Neurotoxicology 27:628–634.

Karen DJ, Li W, Harp PR, Gillette JS, Bloomquist JR. 2001. Striatal dopaminergic pathways as a target for the insecticides permethrin and chlorpyrifos. Neurotoxicology 22:811–817.

Kaufman MH. 1995. The Atlas of Mouse Development. San Diego: Academic Press. 158 p.

Kim IY, Shin JH, Kim HS, Lee SJ, Kang IH, Kim TS, Moon HJ, Choi KS, Moon A, Han SY. 2004. Assessing estrogenic activity of pyrethroid insecticides using in vitro combination assays. J Reprod Dev 50:245–255.

Kojima M, Fukunaga K, Sasaki M, Nakamura M, Tsuji M, Nishiyama T. 2005. Evaluation of estrogenic activities of pesticides using an in vitro reporter gene assay. Int J Environ Health Res 15:271–280.

Lu H, Lim B, Poo MM. 2009. Cocaine exposure in utero alters synaptic plasticity in the medial prefrontal cortex of postnatal rats. J Neurosci 29:12664–12674.

Masuya H, Inoue M, Wada Y, Shimizu A, Nagano J, Kawai A, Inoue A, Kagami T, Hirayama T, Yamaga A, Kaneda H, Kobayashi K, Minowa O, Miura I, Gondo Y, Noda T, Wakana S, Shiroishi T. 2005. Implementation of the modified-SHIRPA protocol for screening of dominant phenotypes in a large-scale ENU mutagenesis program. Mamm Genome 16:829–837.

McCarthy AR, Thomson BM, Shaw IC, Abell AD. 2006. Estrogenicity of pyrethroid insecticide metabolites. J Environ Monit 8:197–202.

Meyer DA, Carter JM, Johnstone AF, Shafer TJ. 2008. Pyrethroid modulation of spontaneous neuronal excitability and

neurotransmission in hippocampal neurons in culture. Neurotoxicology 29:213–225.

Miyamoto J. 1976. Degradation, metabolism and toxicity of synthetic pyrethroids. Environ Health Perspect 14:15–28.

Morgan MK, Sheldon LS, Croghan CW, Jones PA, Chuang JC, Wilson NK. 2007. An observational study of 127 preschool children at their homes and daycare centers in Ohio: Environmental pathways to cis- and trans-permethrin exposure. Environ Res 104:266–274.

Naeher LP, Barr DB, Rithmire N, Edwards J, Holmes AK, Needham LL, Rubin CS. 2009. Pesticide exposure resulting from treatment of lice infestation in school-aged children in Georgia. Environ Int 35:358–362.

Narahashi T. 1996. Neuronal ion channels as the target sites of insecticides. Pharmacol Toxicol 79:1–14.

Nasuti C, Cantalamessa F, Falcioni G, Gabbianelli R. 2003. Different effects of Type I and Type II pyrethroids on erythrocyte plasma membrane properties and enzymatic activity in rats. Toxicology 191:233–244.

Nasuti C, Falcioni ML, Nwankwo IE, Cantalamessa F, Gabbianelli R. 2008. Effect of permethrin plus antioxidants on locomotor activity and striatum in adolescent rats. Toxicology 251:45–50.

Neta G, Goldman LR, Barr D, Sjodin A, Apelberg BJ, Witter FR, Halden RU. 2010. Distribution and determinants of pesticide mixtures in cord serum using principal component analysis. Environ Sci Technol 44:5641–5648.

Neta G, Goldman LR, Barr D, Apelberg BJ, Witter FR, Halden RU. 2011. Fetal exposure to chlordane and permethrin mixtures in relation to inflammatory cytokines and birth outcomes. Environ Sci Technol 45:1680–1687.

Raffetto JD, Khalil RA. 2008. Matrix metalloproteinases in venous tissue remodeling and varicose vein formation. Curr Vasc Pharmacol 6:158–172.

Rogers DC, Peters J, Martin JE, Ball S, Nicholson SJ, Witherden AS, Hafezparast M, Latcham J, Robinson TL, Quilter CA, et al. 2001. SHIRPA, a protocol for behavioral assessment: Validation for longitudinal study of neurological dysfunction in mice. Neurosci Lett 306:89–92.

Seamans JK, Yang CR. 2004. The principal features and mechanisms of dopamine modulation in the prefrontal cortex. Prog Neurobiol 74:1–58.

Semenza GL. 2007. Vasculogenesis, angiogenesis, and arteriogenesis: Mechanisms of blood vessel formation and remodeling. J Cell Biochem 102:840–847.

Shafer TJ, Rijal SO, Gross GW. 2008. Complete inhibition of spontaneous activity in neuronal networks in vitro by deltamethrin and permethrin. Neurotoxicology 29:203–212.

Sleijfer S, Kruit WH, Stoter G. 2004. Thalidomide in solid tumours: The resurrection of an old drug. Eur J Cancer 40: 2377–2382.

Tabernero J. 2007. The role of VEGF and EGFR inhibition: Implications for combining anti-VEGF and anti-EGFR agents. Mol Cancer Res 5:203–220.

Tseng KY, Lewis BL, Hashimoto T, Sesack SR, Kloc M, Lewis DA, O'Donnell P. 2008. A neonatal ventral hippocampal lesion causes functional deficits in adult prefrontal cortical interneurons. J Neurosci 28:12691–12699.

Tulve NS, Jones PA, Nishioka MG, Fortmann RC, Croghan CW, Zhou JY, Fraser A, Cavel C, Friedman W. 2006. Pesticide measurements from the first national environmental health survey of child care centers using a multi-residue GC/MS analysis method. Environ Sci Technol 40:6269–6274.

Yancopoulos GD, Klagsbrun M, Folkman J. 1998. Vasculogenesis, angiogenesis, and growth factors: Ephrins enter the fray at the border. Cell 93:661–664.

In Vitro Cell.Dev.Biol.—Animal
DOI 10.1007/s11626-013-9715-0

LETTER TO THE EDITOR

Primary fibroblast cultures and karyotype analysis for the olive ridley sea turtle (*Lepidochelys olivacea*)

Tomokazu Fukuda · Masafumi Katayama · Kodzue Kinoshita · Takashi Kasugai · Hitoshi Okamoto · Kiyoshige Kobayashi · Masanori Kurita · Makoto Soichi · Kenichiro Donai · Takafumi Uchida · Manabu Onuma · Hideko Sone · Emiko Isogai · Miho Inoue-Murayama

Received: 26 September 2013 / Accepted: 16 November 2013 / Editor: T. Okamoto

Dear Editor

The number of sea turtles in the wild is decreasing because of human activities, such as fishery bycatch (Peckham et al. 2007), oil spills, and marine pollution (Witherington 2001). Furthermore, illegal hunting for their oil, meat, and shells are still continuing (Koch et al. 2013). Hence, protection measures are being implemented in various countries to conserve the endangered species of sea turtles.

In the past few decades, a major concern regarding sea turtles in the wild has been hybridization. Interspecific hybridization has been reported in several areas of the world (Karl et al. 1995; Barber et al. 2003; Lara-Ruiz et al. 2006). The original sea turtle species, such as hawksbill, loggerhead, and olive ridley, had established as independent species for more than millions of years despite overlaps among their habitats (Bowen et al. 1993). However, recent reports on intensive hybridization among these species clearly indicate that these unique original species are at a high risk of extinction in the near future. Acquiring information about the basic genetic background of these species, such as karyotype, is necessary to understand the cause of this intensive hybridization. In this study, we established a primary culture from olive ridley sea turtles and determined the karyotype of the primary cells.

Since 1976, the San Diego Zoo started the preservation of biological specimens derived from critically endangered species in order to facilitate the use of these specimens as research materials for the following generations; this project was named "Frozen Zoo." The significance of this project was internationally recognized, and similar projects, such as the Frozen Ark project in the UK, are underway. The establishment of cell cultures from critically endangered animals might contribute to these cryopreservation projects by increasing the stability of cryopreserved materials and facilitating efficient expansion of cultured cells. Since cultured cells have intact genetic information of the critically endangered animals, the cells have a potential to be used for the genetic analysis of future generations.

The olive ridley sea turtles were maintained at the Port of Nagoya Public Aquarium. Small (3×3 mm) dermal tissue biopsy specimens were obtained from the flipper-like fin of two olive ridley sea turtles. The tissue biopsy specimens were immediately immersed in the cell culture medium. The biopsy process was supervised by a veterinary doctor of the Port of Nagoya Public Aquarium. For the primary culture, a six-well cell culture dish was coated with type I collagen. The detailed method for collagen coating has been described in our previous study (Fukuda et al. 2012). The cell culture was maintained at 26°C under 5% CO_2 in a humidified chamber

T. Fukuda (✉) · M. Katayama · K. Donai · T. Uchida · E. Isogai
Graduate School of Agricultural Science, Tohoku University,
1-1 Tsutsumidori-Amamiyamachi Aoba-ku, Sendai 981-8555, Japan
e-mail: tomofukuda@bios.tohoku.ac.jp

M. Katayama · K. Kinoshita
Japan Society for the Promotion of Science (JSPS), Tokyo, Japan

K. Kinoshita · M. Inoue-Murayama
Wildlife Research Center, Kyoto University, Kyoto, Japan

T. Kasugai · H. Okamoto · K. Kobayashi · M. Kurita · M. Soichi
Port of Nagoya Public Aquarium, Nagoya, Japan

M. Onuma
Ecological Genetics Analysis Section, Center for Environmental Biology and Ecosystem, National Institute for Environmental Studies, Tsukuba, Ibaraki, Japan

H. Sone
Environmental Exposure Research Section, Center for Environmental Risk Research, National Institute for Environmental Studies, Tsukuba, Ibaraki, Japan

Published online: 06 December 2013

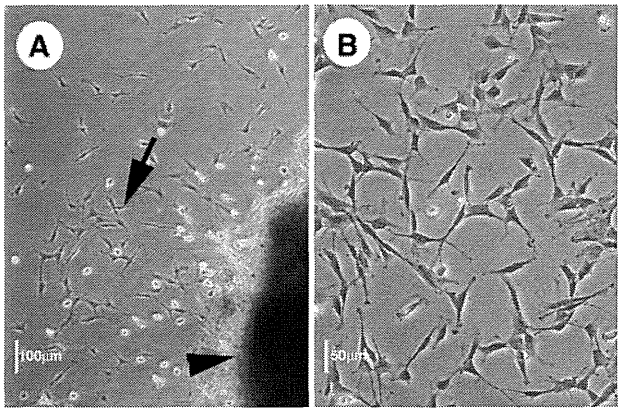

Figure 1. Cell morphology of primary cells obtained from olive ridley sea turtles. *A*, Low-magnification image of primary cell cultures observed 7 d after the start of cell culture. The *arrowhead* indicates the primary tissue, and the *arrow* indicates the growing primary cells. *B*, High-magnification image of primary cells obtained from olive ridley sea turtles.

containing RPMI1640 medium supplemented with 10% fetal calf serum (FCS) and antibiotics in 1× final concentration (Nacalai Tesque, Inc., Kyoto, Japan; product code, 02892-54). The medium was replaced twice per week. The cells were treated with 0.5% trypsin when they reached confluence and were passaged in five-fold dilutions at each passage. For cryopreservation of cells, we used a cryoprotective medium (Cell Banker, Mitsubishi Chemical Medience, Tokyo, Japan), according to the manufacturer's protocol. The detailed method for karyotype analysis has been described in our previous study (Fukuda et al. 2012).

Primary cells from the olive ridley sea turtle specimens were observed 1 wk after the start of cell culture (Fig. 1*A*). The proliferation speed of cells was relatively slow in comparison with that of cells from mammalian species such as mouse or cattle. The primary cells were treated with 0.5% trypsin and passaged into a 100-mm cell culture plastic dish, as described previously (Fukuda et al. 2012). After the cell passages, spindle-shaped primary cells were formed, indicating that these cells could be dermal tissue-derived fibroblasts (Fig. 1*B*).

The karyotype of olive ridley sea turtles was then determined using the primary cells obtained from the primary cell culture. The results of the analysis showed that olive ridley sea turtles have a 2n=56 karyotype, which is exactly the same as that of hawksbill sea turtles (Fig. 2*A–C*) (Fukuda et al. 2012). Karyotype analysis was conducted using two independent primary cells from two olive ridley sea turtles, and a total of 119 metaphase cells were analyzed. Of these 119 cells, 100 (84% diploid) showed a 56 chromosome pattern.

An increased rate of hybridization among sea turtle species has been reported in several areas of the world (Karl et al. 1995; Lu et al. 2000; Barber et al. 2003). Lara-Ruiz et al. (2006) reported on extensive hybridization among hawksbill, loggerhead, and olive ridley sea turtles in Brazil (Lara-Ruiz et al. 2006). Although sea turtle strains have been established as independent species for millions of years, intensive hybridization among multiple species of sea turtles in the past few decades indicates that the pure strains of sea turtles are at a high risk of extinction in the near future. In this study, we established a primary cell line and showed that olive ridley sea turtles have a chromosome number of 2n=56, which is

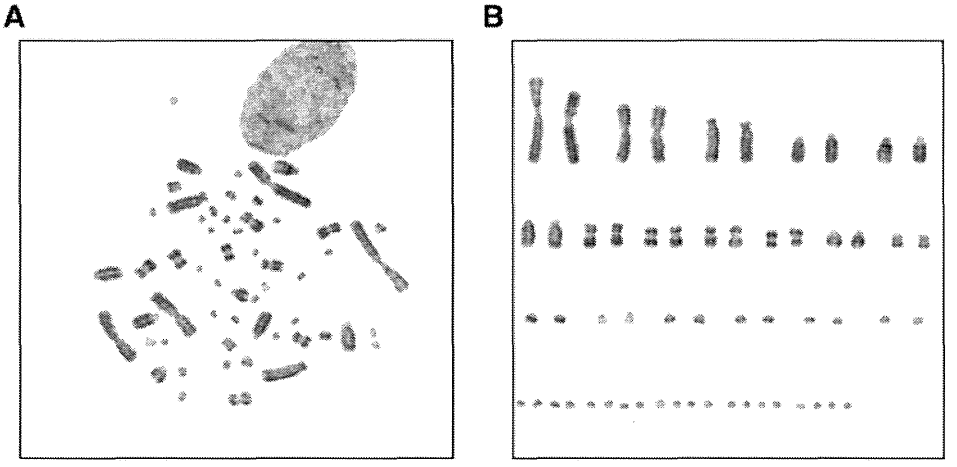

C

Primary ID	Diploid/Total	chromosome number			
		55	56	57	58
Hime L01	50/58 (86%)	7	50	1	ND
Hime L05	51/61 (83%)	10	50	ND	1

Figure 2. Chromosome analysis of the primary cells from olive ridley sea turtles. *A*, Representative metaphase spreads from the primary cells established from olive ridley sea turtles. *B*, Representative aligned karyotype of primary cells. The results revealed a karyotype of 2n=56. *C*, Detailed results of the chromosome analysis. Two primary cells were analyzed. The number of diploid cells per total cells is shown. The cell number that showed variation in chromosome number is listed. *ND* means not detected.

identical to that of hawksbill sea turtles (Fukuda et al. 2012) and loggerhead sea turtles (Fukuda. et al., unpublished data); this finding indicates that hawksbill, loggerhead, and olive ridley sea turtles have the same chromosome number, 2n=56. Since variations in the chromosome structure and number are the factors that restrict chromosome stability, if the chromosome number is different among hawksbill and other sea turtles, it would have been difficult for them to produce stable offspring after hybridization. Our findings indicate that intercrossing between species probably occurs under natural conditions. We showed that recent intensive hybridization among sea turtle species occurred because of the identical chromosome pattern. These findings suggest that the original pure strains of sea turtles might soon become extinct.

The karyotype of the olive ridley sea turtle was first reported in 1986 by Bhunya et al. who established the culture from primary spleen cells (Bhunya and Mohanty-Hejmadi 1986). They reported that olive ridley sea turtles have a karyotype of 2n=56 (Bhunya and Mohanty-Hejmadi 1986). In this study, we obtained identical results. In the case of Reptilia, the determination of karyotype from total blood is difficult, since erythrocytes have nuclei. Bhunya et al. killed olive ridley sea turtles and used their spleen tissues for karyotyping. In this study, small pieces of skin tissue (around 3 mm×3 mm) were found to be enough to initiate cell culture. This study showed that the cell culture method is useful for the determination of karyotype in Reptilia.

We previously reported on the successful establishment of cell culture from hawksbill turtles, and this study reports on the culturing method of primary cells from olive ridley sea turtles. These sea turtles belong to Reptilia, which includes lizards. Unlike lizards, turtles have unique characteristics, such as a carapace. The turtle genome was recently evolutionally analyzed, and turtles were reported to be genetically closer to birds than to lizards (Wang et al. 2013). For performing genomic analyses of critically endangered animals, the preservation of biological specimens is important. The cultured cells contain all the genetic information, such as the nuclear genome, mitochondrial DNA, and micro- and noncoding RNAs. Our established method for the primary turtle cell culture might be useful for the genomic analysis of future generations of olive riddle sea turtles.

Results of mitochondrial DNA analysis have shown that the current species of sea turtles were established around 10 million years ago (Bowen et al. 1993). Elucidating how sea turtles have maintained their genetic independency during the long period of evolution and understanding why sea turtles need to increase their hybridization ratio in past decay are necessary.

Acknowledgments We are grateful to all the members of the team responsible for maintaining the turtle colony at the Port of Nagoya Public Aquarium for their essential help in this study. This work was supported by a collaborative research grant from the Wildlife Research Center of Kyoto University, Japan, and a research grant from the Japan Society for the Promotion of Science (JSPS) KAKENHI (grant numbers 25290082 and 25640117). The founders of the research grant have no role in the research and data analysis. The authors declare that they do not have any conflicts of interest.

References

Barber R. C.; Tontaine C. T.; Flanagan J. P.; Louis E. E. Natural hybridization between a Kemp's ridley (*Lepidochelys kempii*) and loggerhead sea turtle (*Caretta caretta*) confirmed by molecular analysis. *Chelonian Conservation Biol* 4(3): 701–704; 2003.

Bhunya S. P.; Mohanty-Hejmadi P. Somatic chromosome study of a sea turtle, *Lepidochelys olivacea* (Chelonia, Reptilia). *Chromosom Infor Serv* 40: 12–14; 1986.

Bowen B. W.; Nelson W. S.; Avise J. C. A molecular phylogeny for marine turtles: trait mapping, rate assessment, and conservation relevance. *Proc Natl Acad Sci U S A* 90(12): 5574–5577; 1993.

Fukuda T.; Kurita J.; Saito T.; Yuasa K.; Kurita M.; Donai K.; Nitto H.; Soichi M.; Nishimori K.; Uchida T.; Isogai E.; Onuma M.; Sone H.; Oseko N.; Inoue-Murayama M. Efficient establishment of primary fibroblast cultures from the hawksbill sea turtle (*Eretmochelys imbricata*). *Vitro Cell Dev Biol Anim* 48(10): 660–665; 2012. doi: 10.1007/s11626-012-9565-1.

Karl S.; Bowen B.; Avise J. Hybridization among the ancient mariners: characterization of marine turtle hybrids with molecular genetic assays. *J Hered* 86: 262–268; 1995.

Koch V.; Peckham H.; Mancini A.; Eguchi T. Estimating at-sea mortality of marine turtles from stranding frequencies and drifter experiments. *PLoS One* 8(2): e56776; 2013. doi:10.1371/journal.pone.0056776.t001.

Lara-Ruiz P.; Lopez G. G.; Santos F. R.; Soares L. S. Extensive hybridization in hawksbill turtles (*Eretmochelys imbricata*) nesting in Brazil revealed by mtDNA analyses. *Conserv Genet* 7(5): 773–781; 2006. doi:10.1007/s10592-005-9102-9.

Lu Y.; Aguirre A. A.; Work T. M.; Balazs G. H.; Nerurkar V. R.; Yanagihara R. Identification of a small, naked virus in tumor-like aggregates in cell lines derived from a green turtle, *Chelonia mydas*, with fibropapillomas. *J Virol Methods* 86(1): 25–33; 2000.

Peckham S. H.; Maldonado Diaz D.; Walli A.; Ruiz G.; Crowder L. B.; Nichols W. J. Small-scale fisheries bycatch jeopardizes endangered Pacific loggerhead turtles. *PLoS One* 2(10): e1041; 2007. doi:10.1371/journal.pone.0001041.

Wang Z.; Pascual-Anaya J.; Zadissa A.; Li W.; Niimura Y.; Huang Z.; Li C.; White S.; Xiong Z.; Fang D.; Wang B.; Ming Y.; Chen Y.; Zheng Y.; Kuraku S.; Pignatelli M.; Herrero J.; Beal K.; Nozawa M.; Li Q.; Wang J.; Zhang H.; Yu L.; Shigenobu S.; Liu J.; Flicek P.; Searle S.; Kuratani S.; Yin Y.; Aken B.; Zhang G.; Irie N. The draft genomes of soft-shell turtle and green sea turtle yield insights into the development and evolution of the turtle-specific body plan. *Nat Genet* 45(6): 701–706; 2013. doi:10.1038/ng.2615.

Witherington B. Ecology of neonate loggerhead turtles inhabiting lines of downwelling near a Gulf Stream front. *Mar Biol* 140: 843–853; 2001.

Analytical Biochemistry 443 (2013) 104–112

Contents lists available at ScienceDirect

Analytical Biochemistry

journal homepage: www.elsevier.com/locate/yabio

Establishment of a reporter system to monitor silencing status in induced pluripotent stem cell lines

Kenichiro Donai [a], Kengo Kuroda [a], Yijie Guo [a], Kyoung-Ha So [a], Hideko Sone [b], Masayuki Kobayashi [c], Katsuhiko Nishimori [a], Tomokazu Fukuda [a,*]

[a] Graduate School of Agricultural Science, Tohoku University, Aoba-ku, Sendai 981-8555, Japan
[b] Health Risk Research Section, Center for Environmental Risk Research, National Institute for Environmental Studies, Tsukuba, Ibaraki 305-8506, Japan
[c] Graduate School of Bioresource Sciences, Akita Prefectural University, Shimoshinjo, Akita 010-0195, Japan

ARTICLE INFO

Article history:
Received 9 March 2013
Received in revised form 22 July 2013
Accepted 4 August 2013
Available online 21 August 2013

Keywords:
Induced pluripotent stem cells
Gene silencing
Reprogramming
Reporter system

ABSTRACT

Induced pluripotent stem (iPS) cells have proven to be an effective technology in regenerative medicine; however, the low efficiency of reprogramming is a major obstacle to the successful generation of iPS cell lines. One of the most important characteristics of a high-quality iPS cell line is the inactivation of transgenes driven by a retrovirus-derived long terminal repeat promoter. In this study, we established a novel marker system containing three kinds of proteins: secreted-type luciferase (MetLuc), copepod *Pontellina plumata* green fluorescent protein (copGFP), and an antibiotic-resistant gene product (Neo^r). The introduction of MetLuc–copGFP–Neo^r in mouse embryonic fibroblasts (MEFs) allowed us to monitor the reporter expression changes as an indicator of the state of silencing during reprogramming. Transformation of iPS cells induced a remarkable reduction in reporter activity, indicating that the retroviral silencing was detected successfully. Our system enables us to monitor the silencing status of transgenes and to efficiently select iPS cell lines that can be used for further applications.

Reprogramming of human and mouse fibroblasts to generate induced pluripotent stem (iPS)[1] cell lines has been achieved by the expression of only four transcription factors: Oct4, Sox2, Klf4, and c-Myc. These were subsequently referred to as the "four factors" [1–4]. Such iPS cell lines have major potential in the study and therapy of human diseases. This is because they are capable of self-renewal and can give rise to all three primary germ layers: ectoderm, mesoderm, and endoderm. Thus, they are very similar to embryonic stem (ES) cells. However, several fundamental questions of the biology of iPS cells are still unresolved. For example, the mechanisms of genomic reprogramming with the four factors are poorly understood. During this process, continuous expression of the four exogenous transcription factors causes epigenetic changes in the genome, leading to the reactivation of endogenous stem cell-related genes [5]. This results in a dramatic change from a terminally differentiated cell into a stem cell [6–8]. However, the efficiency of this reprogramming process is low; only a few cells can change into iPS cells successfully. It is not clear why the efficiency of this process is so poor. Several studies indicated that iPS cells might be established by an incidental unknown cellular reaction, but this hypothesis on the reprogramming process is still under discussion [9–12].

Because of the low efficiency of iPS cell generation, there are large biological variations in iPS cells compared with ES cells [13,14]. For example, some iPS cells are fully reprogrammed, but some are not. One of the indicators of reprogramming is the silencing of introduced transgenes driven by the retrovirus-derived long terminal repeat (LTR) promoter. In general, these are transcriptionally silenced at a high frequency in "superior" iPS cells during the reprogramming process [2]. As supporting evidence that retroviral silencing is a good indicator of successful reprogramming, Ramos-Mejia and coworkers reported that iPS cells show chromosome abnormalities when the transgene is not well silenced [15]. Furthermore, iPS cells exhibit longer and more stable passages when the retroviral transgene is silenced at an early passage number [16]. The quality of iPS and ES cells is mainly determined by chromosome analysis and/or morphology of the cells, which requires much effort and technical skill.

In this study, we designed a reporter cassette containing three types of markers: MetLuc [17], copepod *Pontellina plumata* green

* Corresponding author. Fax: +81 22 717 8695.
E-mail address: tomofukuda@bios.tohoku.ac.jp (T. Fukuda).

[1] *Abbreviations used:* iPS, induced pluripotent stem; ES, embryonic stem; LTR, long terminal repeat; MetLuc, secreted-type luciferase; copGFP, copepod *Pontellina plumata* green fluorescent protein; Neo^r, neomycin-resistant protein; MCS, multiple cloning site; MEF, mouse embryonic fibroblast; DMEM, Dulbecco's modified Eagle's medium; PBS, phosphate-buffered saline; PEI, polyethylenimine; DIC, differential interference contrast; AP, alkaline phosphatase; PCR, polymerase chain reaction; PBST, PBS with Tween 20; DAPI, 4',6-diamidino-2-phenylindole; SSEA, stage-specific embryonic antigen; cDNA, complementary DNA; RT, reverse transcription; mRNA, messenger RNA; qRT–PCR, quantitative real-time PCR; ETn, early transposon.

0003-2697/$ - see front matter © 2013 Elsevier Inc. All rights reserved.
http://dx.doi.org/10.1016/j.ab.2013.08.014

fluorescent protein (copGFP), and neomycin-resistant protein (Neo^r). This system can detect the remaining expression of transduced genes using only the conditioned medium from iPS cell cultures. It offers an effective system for selecting suitable iPS cell lines for further applications.

Materials and methods

Plasmid construction

The reporter gene cassette encoding MetLuc, copGFP, and Neo^r was chemically synthesized and cloned into the multiple cloning site of pJ204 plasmids (more detailed information is available in Supplementary Document 1 of the online supplementary material). This 2347-bp cassette was inserted into the multiple cloning site (MCS) of the pMYs retroviral vector at the *Bam*HI and *Xho*I restriction sites [18]. The STEMCCA–loxP lentiviral vector was kindly provided by Gustavo Mostoslavsky (Boston University School of Medicine) [19].

Cell culture

293T cells and mouse embryonic fibroblasts (MEFs) were cultured in MEF medium: Dulbecco's modified Eagle's medium (DMEM, cat. no. 08459-35, Nacalai Tesque, Kyoto, Japan) supplemented with 10% fetal bovine serum (cat. no. 12483-020, Invitrogen, Carlsbad, CA, USA) and 100× Antibiotic–Antimycotic Mixed Solution (cat. no. 02892-54, Nacalai Tesque). Infected MEFs were selected for 9 days with DMEM containing 5% fetal bovine serum and 1.2 mg ml^{-1} G418. Mouse iPS cells were cultured on MEF feeder cells in mouse iPSC medium: DMEM with 15% Knockout Serum Replacement (cat. no. 10828-028, Invitrogen), 0.22 mM 2-mercaptoethanol (cat. no. 21438-82, Nacalai Tesque), 100× MEM Nonessential Amino Acids Solution (cat. no. 139-15651, Wako Pure Chemical Industries, Osaka, Japan), 100× Antibiotic–Antimycotic Mixed Solution, and 1000× Leukemia Inhibitory Factor (human, recombinant, culture supernatant, cat. no. 125-05603, Wako Pure Chemical Industries). From the end of the infection to selecting colonies, low-molecular-weight compounds—1.5 μM CHIR99021 (cat. no. 163-24001, Wako Pure Chemical Industries), 0.5 μM PD0325901 (cat. no. 13034, Cayman Chemical, Ann Arbor, MI, USA), and 0.5 μM thiazovivin (cat. no. 04-0017, Stemgent, Cambridge, MA, USA)—were also added to the mouse iPSC medium as reprogramming enhancers [20]. The human iPS cell line was maintained on MEF feeder cells in human iPSC medium: DMEM/F12 GlutaMAX (cat. no. 10565-018, Invitrogen) with 15% Knockout Serum Replacement, 0.22 mM 2-mercaptoethanol, 100× MEM Nonessential Amino Acids Solution, 100× Antibiotic–Antimycotic Mixed Solution, and 4 ng ml^{-1} basic fibroblast growth factor. A human iPS cell line (201B7) was provided by the RIKEN BioResource Center through the Project for Realization of Regenerative Medicine and the National BioResource Project of the Ministry of Education, Culture, Sports, Science, and Technology (MEXT, Japan) [21]. MEFs were isolated from the embryonic tissues of C57BL/6JJcl mice (CLEA Japan, Tokyo, Japan) at embryo day 13.5. For feeder cell preparation, confluent MEFs were treated with mitomycin C (cat. no. M0503-2G, Sigma–Aldrich, St. Louis, MO, USA) at a concentration of 10 μg ml^{-1} for 2.25 h and washed twice in phosphate-buffered saline (PBS). Feeder cells were seeded at a density of 2×10^6 cells per plate. The cells used in these experiments were all incubated at 37 °C under 5% CO_2. All cells were trypsinized using 0.05% trypsin (1:10 dilution, cat. no. 35556-44, Nacalai Tesque). Animal experiments and related activities were approved by the Center for Laboratory Animal Research at Tohoku University.

Production of retroviral reporter gene cassette and infection

293T cells were initially plated at a density of 3×10^6 cells per 100-mm dish for viral production. They were transfected with 3 μg of reporter and packaging plasmids (pCL-10A1, IMGENEX, San Diego, CA, USA) complexed with 18 μg of polyethylenimine (PEI, cat. no. 23966, Polysciences, Warrington, PA, USA). After transfection for 48 h, the culture medium was replaced with new medium containing 8.9 μM forskolin. After an additional incubation for 48 h, the supernatant containing the virus was collected and filtered using a 0.45-μm syringe filter unit (cat. no. 17598, Sartorius, Göttingen, Germany) to remove cell debris. Target MEFs were seeded at a density of 1×10^5 cells per well of a 6-well plate. Virus infection was carried out for 48 h with 6 μg of polybrene (cat. no. 17736-44, Nacalai Tesque).

Production of STEMCCA lentiviral vector and infection

The 293T cells were used as retrovirus producer cells with transient transfection of the packaging plasmid and STEMCCA–loxP lentivirus. The detailed method for the transfection and packaging was described in the previous section. Cells in a 100-mm dish were transfected with 2 μg of STEMCCA–loxP and 4 μg of the packaging plasmids (pCAG-HIVgp and pCMV-VSV-G-RSV-Rev, RIKEN BioResource Center), each complexed with 18 μg of PEI. For determining viral concentration, the solution was placed overnight at 4 °C for precipitation after the addition of a 4× virus concentration (32% polyethylene glycol [PEG] 6000, 0.4 M NaCl, and 40 mM Hepes). The virus pellet was obtained by centrifuging at 3500 rpm for 1 h. The virus pellet was suspended in cell culture medium (DMEM + 10% fetal bovine serum) and infected into the target cells with polybrene. The cell culture medium was replaced with mouse iPSC medium after infection.

Microscopy

Cell morphology was evaluated using differential interference contrast (DIC) microscopy with a Nikon Eclipse TS100 microscope fitted with a Nikon digital camera (DS-Fi1, Nikon, Tokyo, Japan).

AP staining

Cells were fixed with 4% paraformaldehyde and then incubated with alkaline phosphatase (AP) staining solution at 37 °C for 10–15 min. The staining solution contains 0.6 mg ml^{-1} Fast Red TR Salt (hemi [zinc chloride] salt, cat. no. F8764, Sigma–Aldrich), 0.1 mg ml^{-1} naphthol phosphate (cat. no. 23821-24, Nacalai Tesque), 0.7 mM *N,N*-dimethylformamide, 0.2 mM $MgCl_2$, and 0.1 mM Tris–HCl (pH 8.5). Positive staining was detected as red deposits stained by Fast Red.

Genomic PCR

Genomic DNA was extracted from cells grown to confluence in 6-well plates with the TaKaRa FastPure DNA Kit (cat. no. 9191, TaKaRa Bio, Shiga, Japan) according to the manufacturer's protocol. Polymerase chain reaction (PCR) was carried out in a mixture containing 2× PCR buffer of KOD-FX, 0.4 mM dNTP, 0.5 U KOD-FX (cat. no. KFX-101, Toyobo, Osaka, Japan), and 0.3 μM of each primer. The sequences of primers are listed in Supplemental Table 1 of the online supplementary material. The PCR was performed under the following conditions: 50 cycles of 10 s denaturing at 98 °C, 30 s of annealing at 60 °C, and 1 min of extension at 68 °C for STEMCCA–loxP amplification; 30 cycles of 10 s denaturing at 98 °C, 30 s of annealing at 60 °C, and 30 s of extension at 68 °C for MetLuc–copGFP–Neo^r amplification. PCR products were

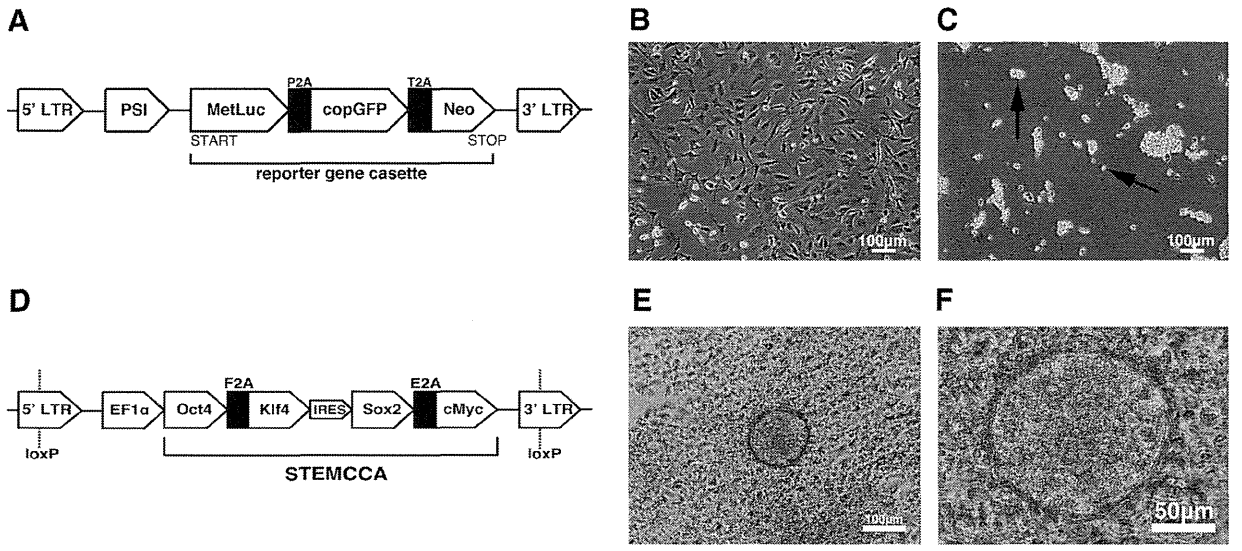

Fig.1. Structure of the expression cassette and induction of the differentiation of induced pluripotent stem (iPS) cells. (A) Structure of the MetLuc reporter retroviral vector. LTR, long terminal repeat; PSI, enhanced packaging signal; MetLuc, a secretory luciferase; copGFP, copepod *Pontellina plumata* green fluorescent protein; Neo^r, neomycin-resistant protein; P2A and T2A, self-cleaving peptides. (B) Mouse embryonic fibroblasts (MEFs) expressing the reporter retrovirus. Note that cells showed G418 resistance after antibiotic selection for 9 days. (C) Control cells with no infection of the reporter retrovirus. Most cells (arrows) showed a rounded phenotype, indicating sensitivity to G418. (D) Structure of the STEMCCA–loxP lentiviral vector containing four reprogramming factors. (E and F) Morphology of a primary iPS colony observed at 16 days after infection with STEMCCA–loxP.

electrophoresed on 1.5% agarose/Tris–acetate–EDTA (ethylenediaminetetraacetic acid) gels and stained with ethidium bromide.

Immunocytochemistry

The iPS cells were fixed with 4% paraformaldehyde in PBS for 15 min and permeabilized with 0.25% Triton X-100 for 30 min. After washing three times in PBS with 0.1% Tween 20 (PBST), cells were blocked with 1% bovine serum albumin in PBS for 1 h and incubated with primary antibodies overnight at 4 °C. After washing three times in PBST, cells were incubated with secondary antibodies and 1 μl of 4′,6-diamidino-2-phenylindole (DAPI) solution (cat. no. 340-07971, Wako Pure Chemical Industries) at room temperature for 1 h. Images of immunofluorescence staining were taken with an Olympus FSX100 fluorescence microscope. The following primary antibodies were used in this study: rabbit anti-mouse Nanog (1:300 dilution, cat. no. RCAB001P, ReproCELL, Kanagawa, Japan), rabbit anti-human Oct3/4 (1:100 dilution, cat. no. SC-9081, Santa Cruz Biochemicals, Dallas, TX, USA), mouse anti-human/mouse stage-specific embryonic antigen (SSEA)-1 (1:100 dilution, cat. no. NL2155R, R&D Systems, Minneapolis, MN, USA), rat anti-mouse/human SSEA-3 (1:100 dilution, cat. no. 09-0014, Stemgent), and mouse anti-human/mouse SSEA-4 (1:100 dilution, cat. no. MAB1435, R&D Systems). The following secondary antibodies were used: Alexa Fluor 594-conjugated goat anti-rabbit IgG (cat. no. A11072) for detecting Nanog, Alexa Fluor 488-conjugated goat anti-rabbit IgG (cat. no. A11070) for detecting Oct3/4, Alexa Fluor 568-conjugated goat anti-mouse IgG (cat. no. A11019) for detecting SSEA-1/SSEA-4, and Alexa Fluor 488-conjugated donkey anti-rat IgG (1:300 dilution, cat. no. A21208, Invitrogen) for detecting SSEA-3.

Luciferase reporter assay

Each mouse iPS cell line was seeded on MEF feeder cells at a density of 5×10^4 per well of a 6-well plate or at 2×10^4 per well of a 12-well plate. Conditioned cultured medium was obtained after 24 h of incubation. Luciferase activities were measured with a Lumat LB 9507 luminometer (Berthold Technologies, Bad Wildbad, Germany) and Ready-to-Glow Secreted Luciferase Reporter Assay (cat. no. 631726, TaKaRa Bio) according to the protocol provided by the manufacturers. Cell counting was done using an automatic cell counter (Countess, Invitrogen).

RT and subsequent quantitative real-time PCR amplification

Total RNA was isolated from cells grown in 6-well plates to confluence using NucleoSpin RNA II kits (cat. no. 740955, TaKaRa Bio). Then, complementary DNA (cDNA) was synthesized with the PrimeScript reverse transcription (RT) reagent kit (Perfect Real Time, cat. no. RR047A, TaKaRa Bio). The manufacturer provides detailed protocols for RNA extraction and cDNA synthesis. Real-time PCR was performed in a 12.5-μl volume containing 2× SYBR Premix Ex Taq II (Tli RNaseH Plus, cat. no. RR820A, TaKaRa Bio), 1 μl of cDNA solution, and 0.4 μM of each primer. The sequences of the primers are available in Supplemental Table 1. Quantitative PCR was performed in triplicate using the Thermal Cycler Dice Real Time System Single (cat. no. TP850, TaKaRa Bio). The standard curve for relative quantitation was obtained from sequential dilution of the cDNA product derived from parental MEFs (for MetLuc–copGFP–Neo^r), mouse ES cells (E14Tg2a for pluripotent markers), and established iPS clone 4 (for STEMCCA–loxP).

Western blot analysis

To obtain a total protein extract, cells were lysed in a solution containing 50 mM Tris–HCl (pH 7.4), 0.15 M NaCl, 1% Triton X-100, 2.5 mg ml^{-1} sodium deoxycholate (cat. no. 194-08311, Wako Pure Chemical Industries), and a protease inhibitor cocktail (1:200 dilution, cat. no. 25955-11, Nacalai Tesque). Cell lysate samples were separated by sodium dodecyl sulfate–polyacrylamide gel electrophoresis and then transferred to hydrophobic polyvinylidene fluoride membranes (cat. no. IPVH00010, Millipore, Billerica, MA, USA). After blocking with 3% nonfat dry milk/PBST, the membranes were probed with anti-neomycin phosphotransferase II (1:1000 dilution, cat. no. 06-747, Millipore) and anti-α-tubulin

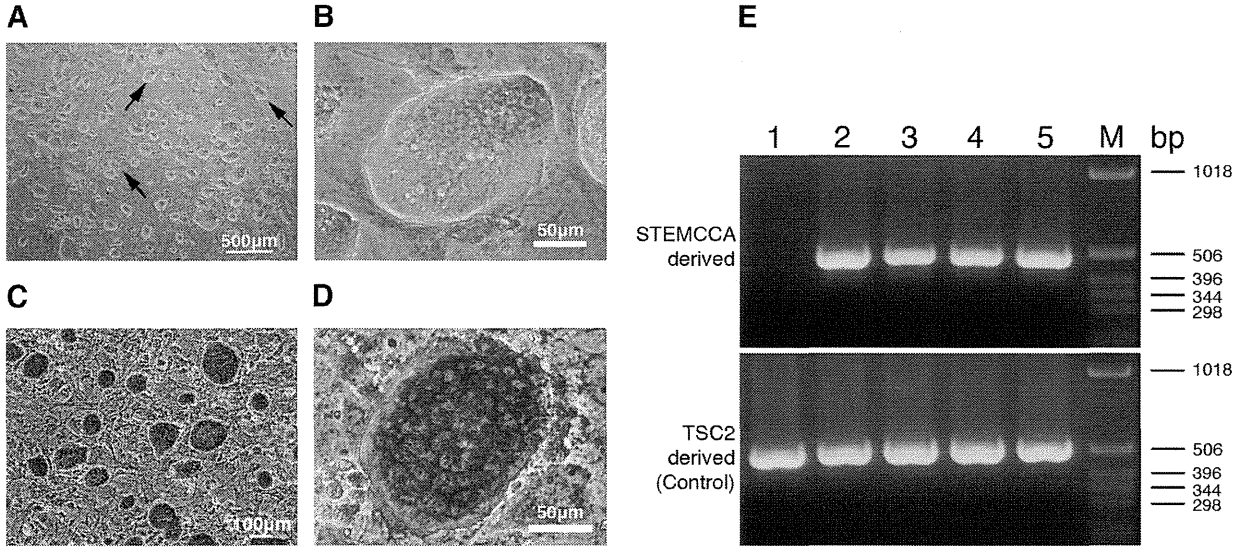

Fig.2. Morphology and genomic characterization of established iPS cell lines. (A and B) Morphology of established iPS lines at passage 6. The arrows indicate iPS colonies. (C and D) Strong positive staining was observed for alkaline phosphatase. (E) Detection of genomic insertion of the STEMCCA–loxP expression cassette by PCR. (Upper panel) All established iPS cell lines showed specific amplification of STEMCCA–loxP (lanes 2–5). No amplification product was recovered from the original ("parental") MEFs (lane 1). (Lower panel) All cells showed a single band from TSC2, serving as an endogenous control. Lane 1: original MEFs; lane 2: iPS clone 2; lane 3: iPS clone 3; lane 4: iPS clone 4; lane 5: iPS clone 5; lane M: 1-Kb DNA ladder; bp, base pairs.

(1:1000 dilution, cat. no. sc-32293, Santa Cruz Biochemicals) antibodies. The blots were then incubated with horseradish peroxidase-conjugated donkey anti-rabbit IgG for detecting anti-neomycin phosphotransferase II with an anti-mouse IgG secondary antibody for detecting α-tubulin (1:2000 dilution, cat. no. NA934V/NA931V, GE Healthcare, Buckinghamshire, UK). Immunoreactive proteins were detected using an ImageQuant LAS-4000 mini (GE Healthcare) with enhanced chemiluminescence (cat. no. RPN2109, GE Healthcare).

Statistical analyses

The results of the luciferase reporter assays and real-time PCR are shown as means with standard deviations. Statistical significance was evaluated using Dunnett's multiple comparison test. Statistical differences were evaluated at $P < 0.05$.

Results

Immortalization of MEFs and introduction of reporter gene cassette

For the efficient detection of retroviral silencing, we focused on the secreted-type luciferase (MetLuc) derived from *Metridia longa* [17]. Because this is released from cultured cells into the medium, lysis of the cells is not required for detection and recovery of the conditioned medium is sufficient. Reporter systems with only fluorescent proteins, such as enhanced green fluorescent protein (EGFP), are not suitable for detection at high sensitivity. Furthermore, such fluorescence is easily saturated, and there is a limitation in achieving linearity of results for quantitation. In conventional methods for the detection of gene expression, such as RT–PCR, we need to lyse the cells for RNA extraction. However, the detection of the secreted-type luciferase in the conditioned medium allows us a time course measurement and high-throughput study with minimal effort.

As shown in Fig. 1A, the reporter gene cassette contains three proteins: MetLuc, copGFP, and Neo^r. These three proteins are conjugated by self-cleavage peptides (P2A and T2A), and the translated protein is expressed under the control of a single promoter. We named this expression cassette MetLuc–copGFP–Neo^r because of its structure. During the initial stage, we immortalized MEFs by introducing E6/E7 oncogenes to retain cell proliferation activity even after antibiotic selection [22]. As expected, E6/E7-expressing MEFs displayed a high proliferation rate and overcame cell senescence in long-term passages (data not shown). We introduced the MetLuc–copGFP–Neo^r cassette into these immortalized MEFs using a retrovirus. Successful infection with MetLuc–copGFP–Neo^r was detected by the expression of copGFP (data not shown). To purify the MEFs that expressed the MetLuc–copGFP–Neo^r cassette, we carried out antibiotic selection with G418. Whereas MEFs expressing the MetLuc–copGFP–Neo^r cassette showed remarkable resistance to G418 (Fig. 1B), immortalized parental MEFs were of round shape and dead, indicating sensitivity to G418 (Fig. 1C). From these results, we conclude that the MetLuc–copGFP–Neo^r cassette was efficiently introduced into E6/E7-immortalized MEFs.

Establishment of mouse iPS cells that express MetLuc–copGFP–Neo^r cassette

We introduced Yamanaka's four reprogramming transcription factors—Oct3/4, Klf4, Sox2, and c-Myc—to induce the formation of iPS cells from MEFs expressing the MetLuc–copGFP–Neo^r cassette. A single lentivirus vector, STEMCCA–loxP, was introduced into MEFs that expressed the MetLuc–copGFP–Neo^r cassette. The characteristic of STEMCCA–loxP is that the four reprogramming factors are incorporated into a single expression vector, which enables highly efficient reprogramming of MEFs into iPS cells (Fig. 1D). Of note, at 21–23 days after infection, we observed dome-shaped colonies that were apparently different from the surrounding MEFs (Fig. 1E and F). We carefully picked out the colonies under a stereomicroscope and examined them. We established four cell lines that showed ES cell-like morphology (Fig. 2A and B). All of the established cell lines showed intense positive staining for AP, one of the markers of pluripotent stem cells (Fig. 2C and D). Furthermore, we detected the STEMCCA–loxP-derived sequence by PCR amplification in all established iPS cell lines but not in the

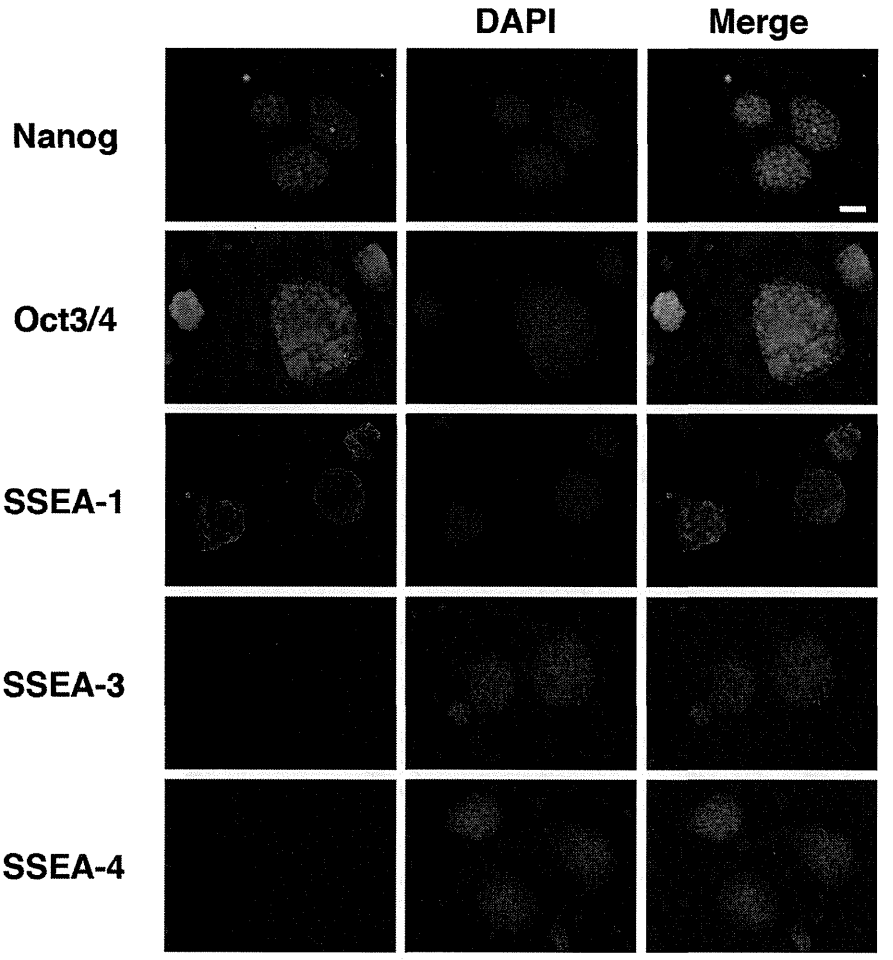

Fig.3. Expression of multiple pluripotent markers in the established iPS cell lines. Nanog- and Oct3/4-positive staining patterns were colocalized at the nucleus, which can be observed as blue counterstaining with DAPI. Stage-specific embryonic antigen (SSEA)-1 protein localizes at the cell surface. White bar = 50 μm. (For interpretation of the references to color in this figure legend, the reader is referred to the Web version of this article.)

parental MEFs, which expressed the MetLuc–copGFP–Neo^r cassette (505 bp, Fig. 2E). Stable amplification with the TSC2-specific primers serving as internal controls for a genomic DNA sequence, is shown in the lower panel of Fig. 2E. From these results, we conclude that the STEMCCA–loxP lentivirus was integrated into the genome of our established stem cell-like cells.

To get further evidence about the nature of our established stem cell-like cells, we confirmed the expression of multiple pluripotent markers—Nanog, Oct3/4, SSEA-1, SSEA-3, and SSEA-4—by immunofluorescence staining (Fig. 3). As shown in Fig. 3, positive staining patterns for Nanog and Oct3/4 were observed, which overlapped well with the nuclear counterstaining with DAPI. SSEA-1 was also detected in our established cell lines, showing as positive staining on the cell surface and junctions. SSEA-3 and SSEA-4 were not detectable. Although our established mouse iPS lines did not show any reactivity for SSEA-3 and SSEA-4, the human iPS cell line showed immunoreactivity to SSEA-3 and SSEA-4 as positive controls [21], indicating that the detection of SSEA markers is fairly reliable (see Supplementary Fig. 1 in online supplementary material). The expression pattern of the pluripotent markers in our established cell lines showed good agreement with that of mouse ES cells. From these observations, we concluded that we successfully established iPS cell lines harboring the MetLuc–copGFP–Neo^r reporter cassette within their genome.

Detection of gene silencing with MetLuc–copGFP–Neo^r cassette by measuring secreted-type luciferase

As mentioned in the introductory paragraphs, the MetLuc–copGFP–Neo^r cassette should be silenced during genomic reprogramming of iPS cells. We first measured luciferase activity of the MetLuc–copGFP–Neo^r cassette in the cell culture medium obtained from our established iPS cell lines. The luciferase activity from the parental MEFs expressing the MetLuc–copGFP–Neo^r cassette is shown in Fig. 4A as a control. Of note, the luciferase activities measured in the condition medium of our established iPS cell lines, clones 2 to 4, showed significant reduction from passage 3 onward. The ratio of the reduction was approximately 1:100 (note that the luciferase activity value is shown on a logarithmic scale). Interestingly, the luciferase activity from the conditioned medium of clone 5 did not show significant reduction when it was compared with that of the control.

To obtain more supportive evidence for the reduced luciferase activity of clones 2 to 4, we evaluated the activity normalized against cell numbers. In brief, the numbers of cells in each clone and corresponding luciferase activity were measured over time (Fig. 4C and D). The numbers of cells of all clones increased from day 1 to day 4, as shown in Fig. 4C. The luciferase activity also increased with time in clones 2 to 4 (Fig. 4D). However, clone 5 showed significantly

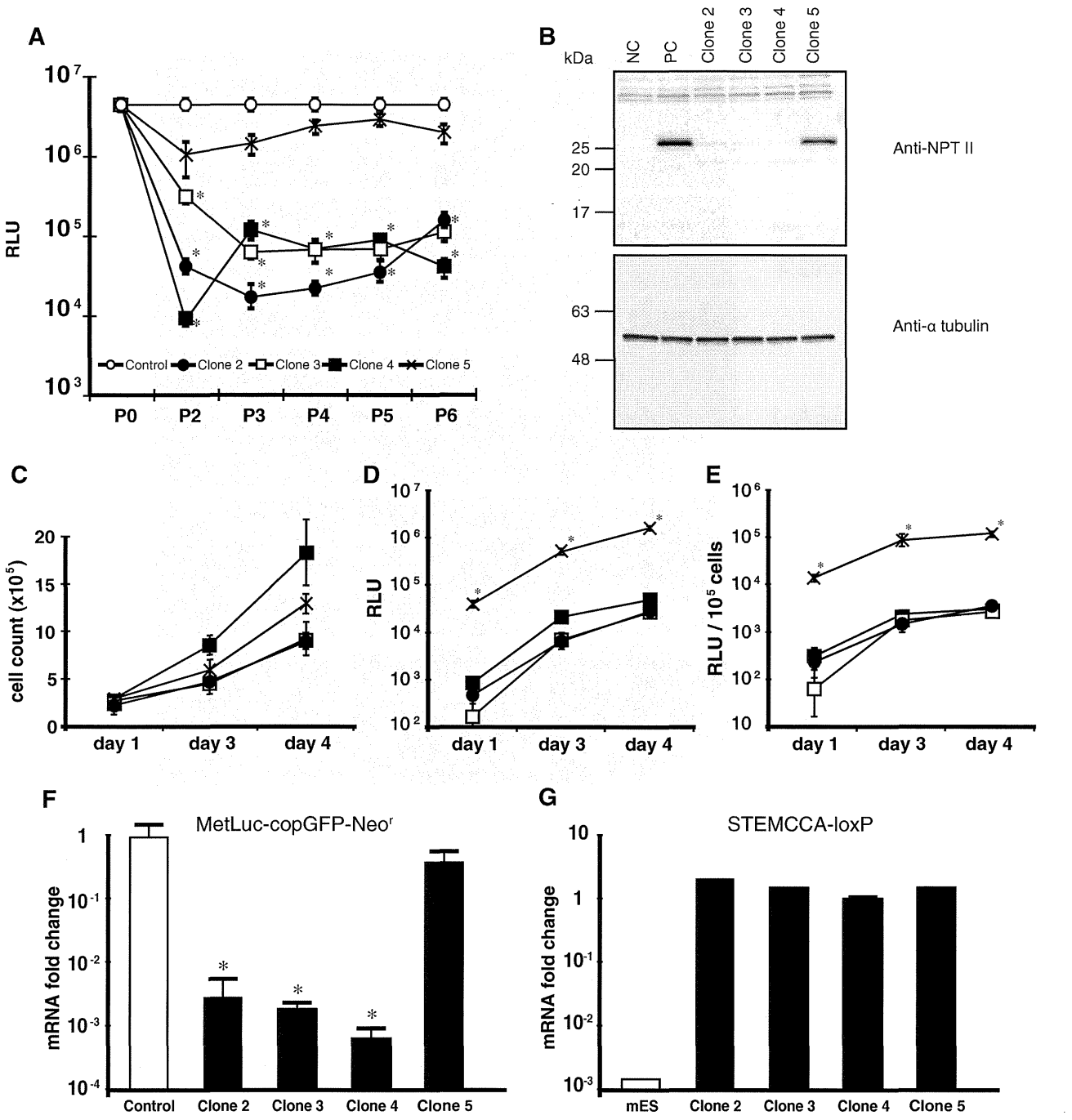

Fig.4. Detection of gene silencing of the introduced expression cassette in established iPS cell lines via luciferase activity, mRNA, and protein levels. (A) Luciferase activity obtained from cultured supernatants after 24 h. The activities in the supernatants from established iPS cell lines and the corresponding controls were compared. Note that clones 2 to 4 showed significantly lower activities than the controls, but clone 5 did not. Statistical significance is indicated by asterisks, and error bars indicate standard deviations (*$P < 0.05$, $n = 6$). RLU, relative light units. (B) Detection of protein expression by Western blotting. (Upper panel) Parental MEFs and clone 5 showed expression of the Neo^r gene. (Lower panel) Each cell line expressed α-tubulin (endogenous control). NC, normal fibroblasts; PC, parental fibroblasts; clones 2 to 5, iPS cells. (C) The cell growth of iPS cells at days 1–4 after the seeding in passage 6. Triplicate samples were detected for each clone. The mean cell numbers and standard deviations are shown. (D) Luciferase activities of conditioned medium at days 1–4 after seeding in passage 6. Clone 5 showed approximately 100 times higher activity than the other clones, as also shown in panel A. Note that the luminescence value is plotted in a logarithmic scale. Error bars indicate standard deviations (*$P < 0.05$). Triplicate samples were tested. (E) Luciferase activities are normalized against cell numbers. The luciferase activity per 10^5 cells at days 1–4 after the seeding are shown. Error bars indicate standard deviations (*$P < 0.05$). (F) mRNA level of MetLuc–copGFP–Neo^r in the parental MEFs and established iPS cells detected by qRT–PCR. A significantly lower level of gene expression was observed in the three established iPS cell lines compared with the parental MEFs. Error bars indicate standard deviations (*$P < 0.05$, $n = 3$). (G) mRNA level of STEMCCA–loxP reprogramming cassette in mouse ES cells and established iPS cell lines detected by qRT–PCR. Fold change is normalized by the expression level of established iPS clone 4 and actin.

higher luciferase activity when compared with clones 2 to 4 through this period (Fig. 4D). The normalized luciferase activity is shown in Fig. 4E. The normalized values of luciferase activities of clones 2 to 4 were significantly lower than in clone 5.